

OXIDATIVE DIMERIZATION OF METHANE OVER LITHIUM-PROMOTED ZINC OXIDE

H.S. Zhang, J.X. Wang, D.J. Driscoll and J.H. Lunsford

Department of Chemistry
Texas A&M University
College Station, TX 77843

INTRODUCTION

The heterogeneously catalyzed oxidative dimerization of methane has received considerable attention in recent years. A variety of materials have now been examined which include the main group oxides (1,2), the rare-earth oxides (3,4) and a number of doped transition (5) and main group metal oxides (6). Work in this laboratory has focused primarily on the latter materials, and in particular Li-doped MgO (7,8). Over this material it is postulated that methane is activated via hydrogen atom abstraction by $[\text{Li}^+\text{O}^-]$ centers which are present under reaction conditions on the surface of the catalyst. Subsequent steps in the mechanism involve the release of these radicals from the surface into the homogeneous gas phase where they then undergo coupling reactions to produce the selective C_2 products.

The formation of $[\text{Li}^+\text{O}^-]$ centers has also been reported on Li-doped ZnO (9,10). This material is considered to be a non-basic semiconductor, whereas, MgO is considered to be a basic insulator. Li-doped ZnO was chosen for examination not only because of its ability to produce potentially active centers, but also to determine the effect of basicity on the catalytic properties. Recent work by Matsuura *et al.* (11) has shown that this material is indeed active for the oxidative dimerization of methane. In the present study, this material will be examined in further detail in an effort to identify the active site on the catalyst surface and to determine the overall mechanism for final product formation.

EXPERIMENTAL

The catalysts were prepared by adding zinc oxide (ZnO) and lithium carbonate (Li_2CO_3) to deionized water and evaporating the water, while stirring, until only a thick paste remained. The paste was dried in air at 140°C overnight. This material was then pressed, broken into small chips, loaded into the reactor and preconditioned at 750°C for 4 h under a flow of oxygen before exposure to the reactant gases. The unpromoted ZnO catalyst was prepared and pretreated in the same manner, except for the addition of Li_2CO_3 .

The catalytic studies were carried out in a conventional fused-quartz flow reactor operated at atmospheric pressure. Typical reactant feeds consisted of a 2:1 methane:oxygen feed diluted with a helium carrier gas at a total flow of 50 ml/min. Reaction temperatures ranged from 600 to 770°C . Product analysis was accomplished by conventional GC techniques. Further details on this system can be found in previous papers by Lunsford and co-workers (3,7).

The EPR spectra were obtained using a Varian E-6S spectrometer at 77 K. Quenching studies were carried out using the technique previously developed in this laboratory by Wang *et al.* (12). In this

work, the samples were quenched into liquid oxygen after exposure to 180 torr of gaseous oxygen at 730°C for 1 h.

RESULTS

Catalyst Preconditioning

The method used to pretreat the catalyst was found to have a strong influence on the reaction stability. Samples preconditioned for 3 h at 650°C in air rapidly deactivated, regardless of the reaction temperature, methane/oxygen ratio or the sample purity. However, by increasing the pretreatment temperature to 750°C and employing a 50 ml/min oxygen flow a steady state could be rapidly attained. In this case, a steady state reaction was achieved after only 2.5 h and was maintained even after 130 h on stream. Therefore, to ensure that all results were obtained after steady state had been reached, samples were pretreated at 750°C for 4 h under an oxygen flow and measurements were not begun until after 12 h on line.

Catalytic Studies

In order to gain insight into the overall reaction mechanism the effects of temperature, Li-doping levels and reactant partial pressures on reactivity were examined in detail. The effect of temperature is considered first and the results are illustrated in Figure 1. Methane conversion continually increased with increasing temperature over the entire range examined. The C₂ selectivity slowly increased to a maximum at a temperature of approximately 675°C while a reverse temperature dependence was observed for the C₁ selectivity. The increase in C₂ selectivity with increasing activity is contrary to expected behavior; however, a similar trend was previously observed during the oxidative dimerization of methane over Li-doped MgO catalysts (7). The activation energy determined for this reaction, over the temperature range of 550 to 700°C was 51 kcal/mol.

The effect of lithium doping was examined and a plot of methane conversion, C₂ selectivity, C₁ selectivity and C₂ yield (which is defined as the product of conversion and selectivity) vs lithium doping into ZnO is presented in Figure 2. Methane conversion reached a maximum over the pure oxide; however, selectivity to C₂ products was extremely low. Addition of lithium resulted in a decrease of methane conversion, but the C₂ selectivity rapidly increased and eventually leveled off at a doping level of approximately 1.0 wt% Li. A corresponding decrease in the C₁ was also observed. The major component in the C₁ fraction was CO₂ (>90%) while the C₂ portion consisted of a mixture of ethane and ethylene at a constant ratio of C₂H₄/C₂H₆ = 0.85. The surface areas of these used materials decreased from 0.5 m²/g over the pure oxide to a constant value of ~0.1 m²/g over all of the lithium-doped samples.

In one experiment a used catalyst was thoroughly washed to remove any residual Li₂CO₃ from the surface. This material exhibited an activity for C₂ formation which was comparable to the original catalyst; however, the rate of C₁ product formation increased considerably.

The variation of reactivity with respect to oxygen partial pressure is presented in Figure 3. This data was obtained over a 0.9 wt% Li/ZnO catalyst at 720°C; however, similar behavior was also observed at a reaction temperature of 660°C. As the oxygen partial pressure was increased, methane conversion continued to increase. At low oxygen partial pressures the formation of selective C₂ products

was favored whereas, as expected, high oxygen partial pressures tended to promote the production of non-selective CO and CO₂.

Maximum C₂ Yields

In order to obtain the maximum C₂ yields catalytic runs were carried out over 4 g of a 0.9 wt% Li/ZnO catalyst at several different temperatures and these results, along with some typical conversion and selectivity data, are summarized in Table I. A maximum C₂ yield of 15% was obtained at a temperature of 750°C. Higher yields apparently could be obtained at higher temperatures; however, at these temperatures the catalyst appeared to enter a molten phase. It is of value to compare these yields with those previously obtained over the Li/MgO catalysts (7). At 720°C under similar reactant feed conditions a C₂ yield of 18% was observed. The value of 11% obtained here at 720°C is obviously lower, but still within the range of the more active methane conversion catalysts thus far reported.

Table I.

MAXIMUM C₂ YIELD

Temperature(°C)		650	700	720	750
Selectivity(%)	CO ₂	44.0	39.6	42.4	43.7
	CO	4.9	1.4	0.0	3.0
	C ₂ H ₄	10.4	22.2	26.9	28.7
	C ₂ H ₆	40.7	36.8	30.7	24.6
	Total C ₂	51.1	59.0	57.6	53.3
Conversion(%)	CH ₄	5.1	13.9	18.7	28.2
	O ₂	11.7	25.3	35.2	55.5
C ₂ Yield(%)		2.6	8.2	10.8	15.0

Catalyst: 4g 0.9 wt% Li/ZnO; Flow rates: He = 42.5 ml/min, CH₄ = 5.0 ml/min, O₂ = 2.5 ml/min.

EPR Studies

Quenching of all of the doped materials from high temperature in the presence of oxygen resulted in the detection of [Li⁺O⁻] centers. No [Li⁺O⁻] signal, or O⁻ signal, was detected over pure ZnO. The variation of [Li⁺O⁻] concentration with respect to lithium doping is presented in Figure 2 along with the selectivity and conversion data obtained under steady state reaction conditions.

DISCUSSION

To simplify presentation of the mechanism it is best to divide the discussion into two sections: (1) methane activation and (2) stable product formation.

Methane Activation

The presence of [Li⁺O⁻] centers in the quenched samples once again suggests that this site is most likely responsible for the initial methane activation. Although the [Li⁺O⁻] concentration curve

does not correlate well with the conversion curve in Figure 2, relatively good agreement is observed with the C_2 yield curve, and there is even better agreement with the C_2 selectivity curve. Furthermore, in the absence of these centers (i.e. over the pure oxide) the formation of both ethane and ethylene is negligible which provides additional support for the fact that $[Li^+O^-]$ centers are required to promote selective C_2 product formation. In accord with the earlier work over Li-doped MgO catalysts it is proposed that methane is activated via hydrogen atom abstraction by $[Li^+O^-]$ centers to produce the methyl radical (7).

Stable Product Formation

The conversion and selectivity data presented in Figure 2 clearly show that selective C_2 product formation is not favored on the pure oxide surface. In addition, as C_2 selectivity increased the surface area of the catalyst fell by a factor of approximately 5. This further suggests that the catalyst surface is not entirely responsible for the selective product formation. In agreement with the earlier Li/MgO work, it is once again proposed that ethane and ethylene are formed via coupling of the radicals in the gas phase and not on the surface (7).

The formation of the non-selective products, CO and CO_2 , is also briefly considered. As mentioned above, reaction on the catalyst surface appears to be a major source for these products. In addition, the data of Figure 1 indicates that the selectivity for these products increases at temperatures greater than approximately 700°C. This is believed to be due to the further oxidation of the C_2 products. This route apparently is only important at these elevated temperatures. High oxygen partial pressures also tends to promote complete oxidation products (Figure 3), but it is not possible to determine whether this is promoted on the surface or in the gas phase from this data.

Lithium carbonate on the surface appears to moderate the non-selective activity of the zinc oxide, but it has no effect on the selective oxidative dimerization reaction. When the carbonate was removed only the non-selective reactions were affected. Since zinc oxide itself is not a strongly basic oxide, one may conclude that basicity is not a prerequisite for the selective reaction.

CONCLUSIONS

The mechanism for the oxidative dimerization of methane over Li-doped ZnO is similar to that previously proposed for the same reaction over Li-doped MgO. Surface-generated gas phase methyl radicals are produced from the interaction of methane with $[Li^+O^-]$ centers. Gas phase coupling reactions provide the primary route for the formation of the selective C_2 products. Non-selective C_1 product formation is most likely promoted on the pure oxide surface. A strongly basic oxide is not required for the selective oxidative dimerization of methane.

ACKNOWLEDGMENTS

This work was supported by the National Science Foundation under Grant No. CHE-8405191.

REFERENCES

1. Keller, G.E. and Bhasin, M.M., *J. Catal.*, 73, 9 (1982).
2. Sofranko, J.A., Leonard, J.J. and Jones, C.A., *J. Catal.*, 103, 302 (1987).
3. Lin, C.H., Campbell, K.D., Wang, J.X. and Lunsford, J.H., *J. Phys. Chem.*, 90, 534 (1986).
4. Otsuka, K., Jinno, K. and Morikawa, A., *J. Catal.*, 100, 353 (1986).
5. Jones, C.A., Leonard, J.J. and Sofranko, J.A., *J. Catal.*, 103, 311 (1987).
6. Ali Emesh, I.T. and Amenomiya, Y., *J. Phys. Chem.*, 90, 4785 (1986).
7. Ito, T., Wang, J.X., Lin, C.H. and Lunsford, J.H., *J. Am. Chem. Soc.*, 107, 5062 (1985); Ito, T. and Lunsford, J.H., *Nature (London)*, 314, 721 (1985).
8. Driscoll, D.J., Martir, W., Wang, J.X. and Lunsford, J.H., *J. Am. Chem. Soc.*, 107, 58 (1985).
9. Haber, J., Kosinski, K. and Rusiecka, M., *Discuss. Faraday Soc.*, 58, 151 (1974).
10. Schirmer, O.F., *J. Phys. Chem. Solids*, 29, 1407 (1968).
11. Matsuura, I., Utsumi, Y., Nakai, M. and Doi, T., *Chem. Lett.*, 1981 (1986).
12. Wang, J.X. and Lunsford, J.H., *J. Phys. Chem.*, 90, 5883 (1986).

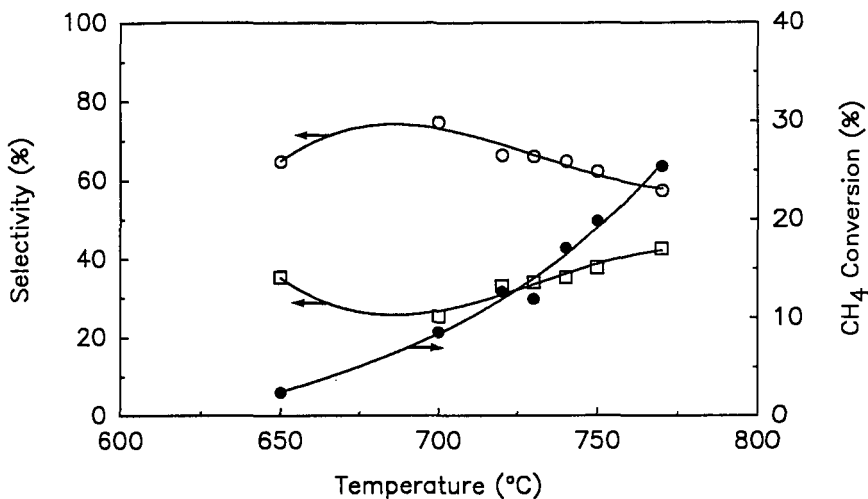


Figure 1. Methane conversion and product selectivity as a function of temperature: ● methane conversion; □ C₁ selectivity; ○ C₂ selectivity. Catalyst: 0.9 wt% Li/ZnO.

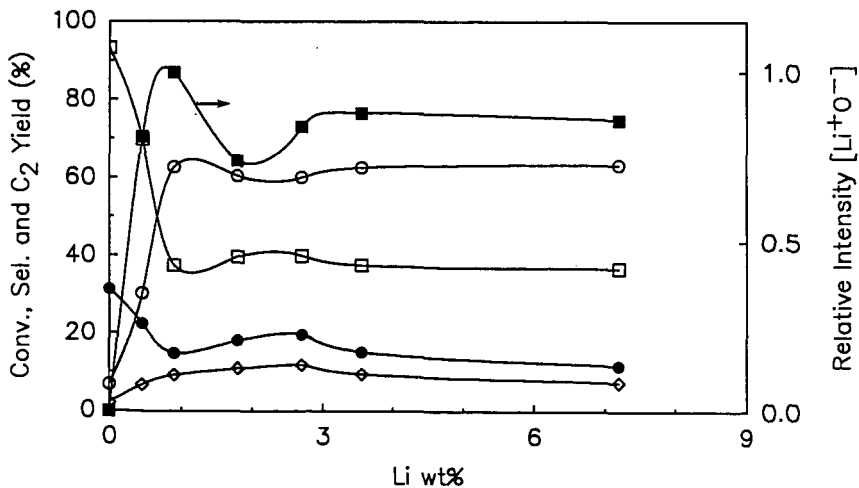


Figure 2. Methane conversion, product selectivity and C₂ yield as a function of Li-doping into ZnO: ● methane conversion; □ C₁ selectivity; ○ C₂ selectivity; ◇ C₂ yield; ■ [Li⁺O⁻] concentration. Temp: 750°C.

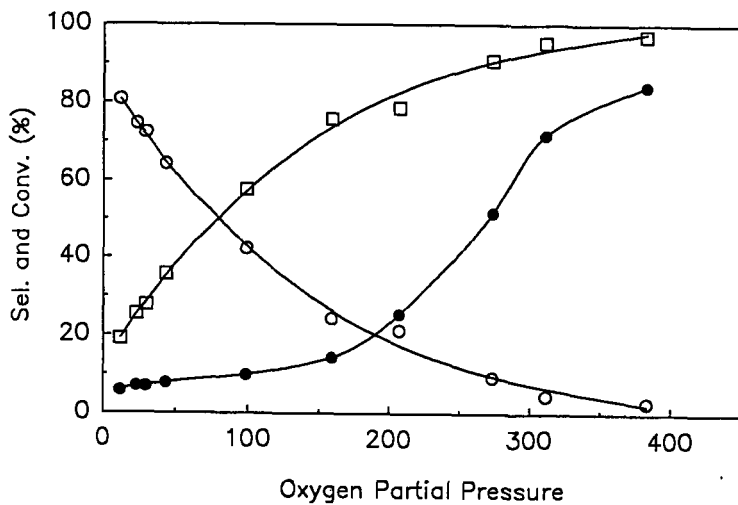


Figure 3. Methane conversion and product selectivity as a function of oxygen partial pressure: ● methane conversion; □ C₁ selectivity; ○ C₂ selectivity. Catalyst: 0.9 wt% Li/ZnO; Temp: 720°C.

CATALYTIC PARTIAL OXIDATION OF METHANE TO HIGHER HYDROCARBONS

R.J. Tyler and C.A. Lukey

CSIRO Division of Fossil Fuels, PO Box 136, North Ryde, NSW 2113, Australia

1. INTRODUCTION

The direct conversion of methane to higher hydrocarbons such as ethylene is currently a very active research area. Olefins are of particular importance as they represent intermediates suitable for oligomerisation to transport fuels. Jones et al. (1) recently reviewed the potential for methane conversion and described results using Mn-based redox type catalysts in both cyclical (using air and methane alternately) and continuous reactors. Bytyn and Baerns (2) reported the activity of PbO-based catalysts and concluded that the acidity of the surface influences the reaction pathway, with high acidity resulting in poor selectivity to the desired hydrocarbons. Otsuka et al. (3,4) described results for a variety of catalysts including rare earths, transition metal elements, alkali and alkaline earth compounds and halide doped mixtures. Lunsford et al. (5,6) were the first to report the use of a Li-doped magnesia and postulate that methane activation occurred at $[Li^+O^-]$ centres. This catalyst is notable in that it does not contain metal ions of variable oxidation state and the active species is thought to involve the anion. A remarkable feature of the published data is the variety of surfaces that promote the reaction and the similarity of many of the reported product distributions. This suggests that after the initiation step the hydrocarbon building steps probably occur via a gas phase mechanism (1).

The present paper reports results obtained using a Li/MgO catalyst with CH_4/O_2 mixtures and describes the influence of contact time and oxygen concentration on reaction rate and product selectivities. Implications for the reaction mechanism are also discussed.

2. EXPERIMENTAL

Catalysts were prepared by procedures similar to those described by Ito and Lunsford (5) and calcined in air at 850°C before use. Initial Li loadings were equivalent to a Li/Mg atomic ratio of 0.58. However subsequent analysis showed substantial loss on firing and to some extent during reaction.

Experiments were conducted using quartz or alumina fixed-bed reactors and a continuous flow of feed gas. Pseudo-contact times (W/F) equivalent to the weight of catalyst (g) divided by the feed gas flowrate at operating conditions ($ml\ s^{-1}$) were varied in the range 0.01 to 2. Temperatures were in the range 550 to 850°C. Exit gas analysis was performed by gas chromatography (hydrocarbons) and continuous gas analysers (CO , CO_2 and O_2). In some experiments water analyses were also carried out enabling oxygen balances to be determined (usually $100 \pm 5\%$) and hydrogen yields to be calculated from a hydrogen balance. Confirmation of hydrogen yields by analysis was obtained in selected experiments.

3. RESULTS AND DISCUSSION

3.1 Reaction rates

Figure 1 shows the dependence of the methane conversion rate ($mmol\ CH_4\ min^{-1}\ g^{-1}$ catalyst) on the pseudo-contact time (W/F) for a range of O_2 concentrations using 17.3 g of catalyst at 770°C. The methane content of the feed gas was held constant at 90% and the oxygen concentration was varied between 1 and 9.4% with the balance being nitrogen.

As expected, the methane conversion rate increased as the level of oxygen in the feed gas increased. However, for each oxygen level there was a marked decline in

methane conversion rate as the contact time increased (i.e. as the gas velocity through the reactor decreased). The possibility that this effect was caused by limitations in the mass transfer of reactants across the boundary layer to the external surface of the catalyst was checked using standard calculation procedures (7). In all cases the reactor was found to be operating well outside the regime where external mass transfer limitations apply. Presumably the observed decline in methane conversion rate with increasing contact time results from operating the reactor in an integral mode where the variation in W/F results in different average reactant and product concentrations and hence different reaction rates. The possibility of rate suppression by one or more of the products reducing catalyst activity must also be considered.

3.2 Methane conversion and product selectivity

Methane conversion (percentage of input methane converted to products), oxygen consumption (percentage of input O_2 consumed) and product selectivity (amount of input methane converted to a specific product as a percentage of total methane converted) for feed gases containing 1.1 and 9.4% O_2 are illustrated in Fig. 2 as a function of W/F. At the lower O_2 concentration (Fig. 2a), total O_2 consumption was achieved at the longest contact time when CH_4 conversion reached 3%. Selectivity to hydrocarbons was very high at 94% for W/F = 0.3, of which 91% corresponded to C_2 hydrocarbons and 3% C_3 hydrocarbons, principally propane. At total O_2 consumption, hydrocarbon selectivity was still high at 93% with C_3 's increasing to 5% and consisting principally of propylene. Increasing contact time resulted in an increasing conversion to ethylene with a corresponding decrease in ethane. Carbon dioxide was the dominant carbon oxide product.

With 9.4% O_2 in the feed gas (Fig. 2b) the selectivity to hydrocarbons showed a strong dependence on contact time, declining from 85% at W/F = 0.3 to 76% at 1.5. C_3 hydrocarbons, mainly propylene, reached 6% at the longer reaction times. The loss in hydrocarbon selectivity appears to be due to an increasing contribution from secondary reactions in the presence of a higher O_2 concentration and is reflected in increasing selectivity to carbon oxides. This is accompanied by an increased production of ethylene and decline in ethane.

Minor yields of other hydrocarbons were observed, including butenes, butadiene and, at higher temperatures, benzene, toluene and acetylene. These products all demonstrate an increasing contribution from secondary gas phase reactions as operating conditions became more severe. Hydrogen was also observed in the product stream in amounts equivalent to about 15% of the hydrogen liberated by the methane conversion and also depended upon reaction severity. Hydrogen could arise by pyrolysis of ethane to ethylene or possibly by decomposition of reaction intermediates such as formaldehyde.

The dependence of CH_4 conversion, O_2 consumption and product selectivity on O_2 concentration in the feed gas is summarised in Fig. 3 for a fixed W/F value of 1.5. Hydrocarbon selectivity declined linearly with increasing O_2 concentration in the feed gas (CH_4 constant at 90%) accompanied by increasing formation of carbon oxides. Ethane selectivity declined rapidly with increasing O_2 concentration whereas ethylene increased and eventually reached a plateau of 42%. In other experiments where total O_2 consumption was achieved, ethylene selectivity reached a maximum and then declined with increasing contact time suggesting that secondary, undesired production of carbon oxides adversely affected ethylene production. O_2 consumption showed a small decrease with increasing O_2 content whereas CH_4 conversion increased markedly, reaching 11% with 9.4% O_2 in the feed gas.

3.3 Reaction sequence

Ito et al. (5,6) proposed that the initial step in the catalytic conversion was the formation of a methyl radical by hydrogen abstraction from a methane molecule at a

thermally generated $[Li^{+}O^{-}]$ site. Recombination of two methyl radicals either on the surface or in the gas phase produced ethane. Ethylene was thought to arise from partial oxidation or pyrolysis reactions of ethane. Carbon oxides arose from either oxidation of methyl radicals or further oxidation of C_2 products.

In an attempt to clarify the reaction sequence, experiments were conducted at short pseudo-contact times using a small catalyst bed (<0.5 g) in order to examine the product distribution at low extents of reaction. Figure 4 shows the dependence on temperature of CH_4 conversion, O_2 consumption and product selectivity at a fixed W/F of 0.05 using a 50% $CH_4/5\% O_2/45\%$ He feed gas mixture. Clearly at temperatures below about $700^{\circ}C$ CH_4 conversion and O_2 consumption were low, C_2 hydrocarbon selectivity was also low and carbon oxides were the major products below about $650^{\circ}C$. Increasing the temperature resulted in increasing C_2 selectivity, which reached a broad maximum of 75% between 750 and $800^{\circ}C$. Below $650^{\circ}C$ ethane was the only hydrocarbon species, with selectivity to ethylene increasing at higher temperatures. These data suggest that, at least in the early stages of the reaction, ethane and carbon oxides are formed by parallel rather than sequential reactions. The reactions involved must have different activation energies, resulting in a changing product distribution with increasing temperature.

Further evidence in favour of this reaction sequence is depicted in Figure 5. These data were derived at short residence times (W/F = 0.01-0.1) with a feed gas consisting of 95% $CH_4/5\% O_2$. Product selectivities are shown as a function of methane conversion, and the diagram includes a curve representing O_2 consumption. At the higher conversions C_2 selectivity started to decline and carbon oxides to increase owing to secondary oxidation as the oxygen consumption approached 100%. However, extrapolation of the selectivities back to zero conversion provides evidence of the primary reaction products without contribution from secondary processes. In this example and in all other experiments only ethane and carbon oxides formed intercepts. Ethylene and C_3 hydrocarbon selectivities extrapolate to zero at zero CH_4 conversion indicating that these products arise from secondary reactions of ethane. The increase in carbon oxides at higher conversion must be associated with further oxidation of product hydrocarbons.

The simultaneous formation of ethane and carbon oxides again suggests that in the early stages of the reaction these products arise from parallel rather than sequential reactions. There is thus no direct route to ethylene. These so-called 'primary selectivities' at zero conversion are considered to be an intrinsic property of the catalyst and as such provide a useful means of comparing the performance of different catalysts.

CONCLUSIONS

Product selectivity from the catalytic partial oxidation of methane over a Li/MgO catalyst is very dependent on contact time, O_2 concentration and temperature. Very high selectivities to hydrocarbons ($>90\%$) can be achieved provided high $CH_4:O_2$ ratios ($>50:1$) are used. The reaction sequence involves the initial formation of ethane and carbon oxides via parallel reactions. There is no direct route to ethylene, which arises from secondary reactions of ethane.

ACKNOWLEDGEMENTS

This study forms part of a larger nationally coordinated program on the direct conversion of methane involving CSIRO, the Melbourne Research Laboratories of The Broken Hill Proprietary Company Ltd. and Australian universities. Funding under the National Energy Research Development and Demonstration Program is gratefully acknowledged. The technical skills of A. McCutcheon and J. Smith contributed significantly to this investigation.

REFERENCES

1. Jones C.A., Leonard J.L. and Sofranko J.A. *Energy Fuels* 1987, 1, 12-16.
2. Bytyn W. and Baerns M. *Appl. Catal.* 1986, 28, 199-207.
3. Otsuka K., Jinno K. and Morikawa A. *J. Catal.* 1986, 100, 353-359.
4. Otsuka K. and Komatsu T. *J. Chem. Soc. Chem. Commun.* 1987, 388-389.
5. Ito T. and Lunsford J.H. *Nature* 1985, 314, 721-722.
6. Ito T., Wang J., Lin C. and Lunsford J.H. *J. Am. Chem. Soc.* 1985, 107, 5062-5068.
7. Edwards J.H., personal communication.

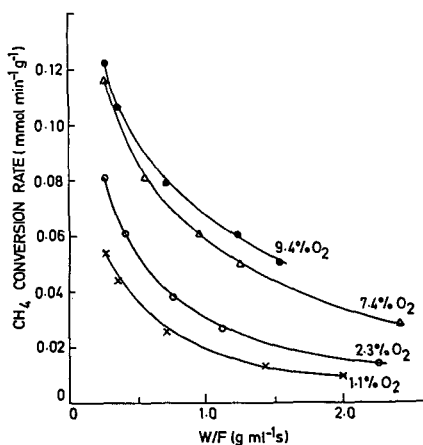


Figure 1. Influence of pseudo-contact time and oxygen level in feed gas on methane conversion rate at 770°C (feed gas 90% CH₄)

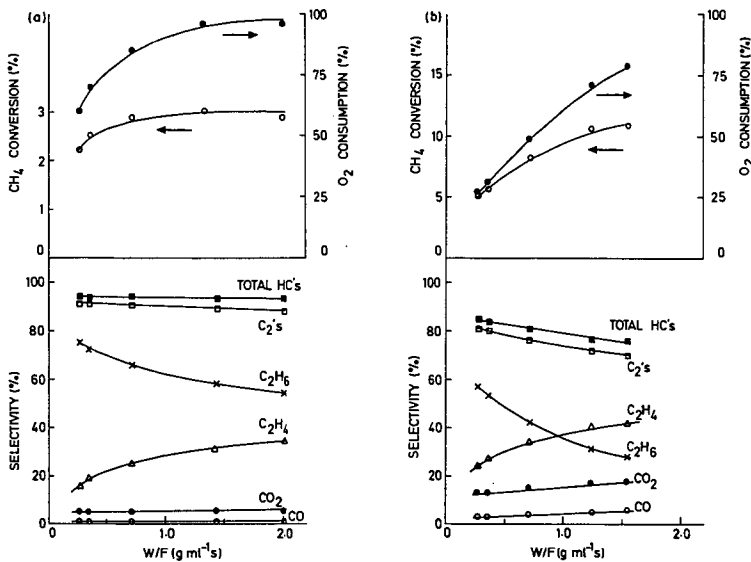


Figure 2. Influence of pseudo-contact time on methane conversion, oxygen consumption and product selectivities at 770°C. (a) Feed gas 1.1% O₂, 90% CH₄. (b) Feed gas 9.4% O₂, 90% CH₄

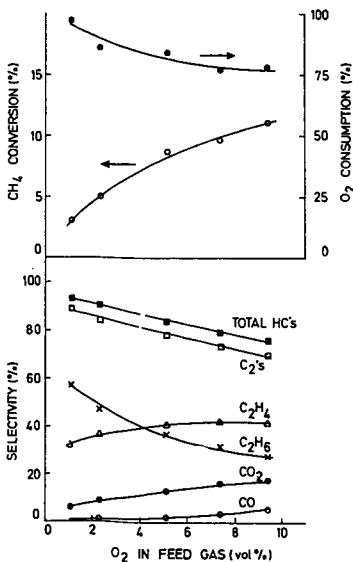


Figure 3. Influence of oxygen level in feed gas on methane conversion, oxygen consumption and product selectivities at 770°C (W/F = 1.5 g ml⁻¹s)

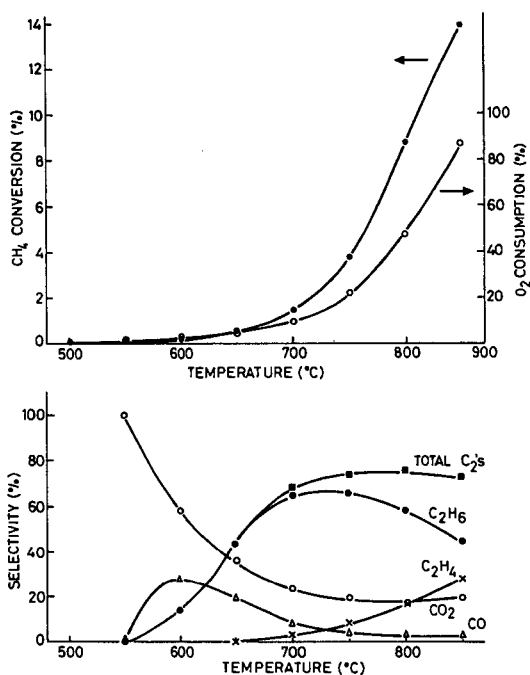


Figure 4. Effect of temperature on methane conversion, oxygen consumption and product selectivity (feed gas 50% CH₄, 5% O₂)

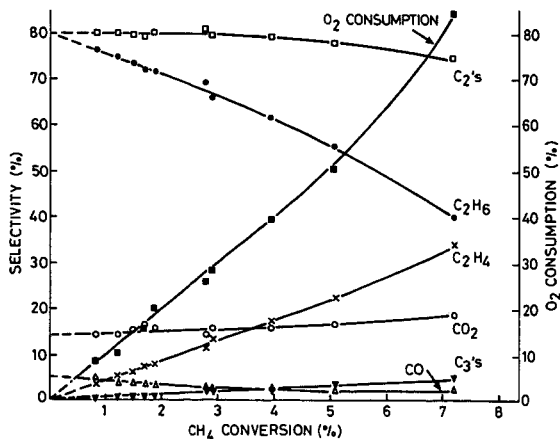


Figure 5. Variation of product selectivity and oxygen consumption with methane conversion at 750°C (feed gas 95% CH₄, 5% O₂)

THE DIRECT CONVERSION OF METHANE TO METHANOL BY A HIGH PRESSURE PARTIAL OXIDATION REACTION

H. D. Gesser, N. R. Hunter, L. A. Morton, P. S. Yarlagadda and D. P. C. Fung*

Department of Chemistry, University of Manitoba, Winnipeg, Manitoba, R3T 2N2 and
*Energy Research Laboratory, CANMET, Department of Energy, Mines and Resources,
Ottawa, K1A 0G1, Canada.

INTRODUCTION

The conversion of methane to a liquid storageable fuel is a desirable alternative to compressed natural gas. The simplest liquid is methanol presently formed by the steam reforming of methane to synthesis gas followed by the high pressure catalytic conversion of the synthesis gas to methanol. The process is most economic for large (2000 tonne/day) plants and must be located near large reserves of natural gas or near an appropriate pipeline. The simpler partial oxidation route offers the advantage of directly converting methane to methanol in a single step reaction. The potential for the partial oxidation route together with an economic evaluation has been reported by Edwards and Foster (1) who showed that, provided the selectivity for methanol formation is about 77%, the partial oxidation route has an economic advantage over the conventional synthesis route with no penalty for conversions as low as 4%.

Much has been published on the combustion of methane to CO_2 and H_2O but very little has been concerned with the intermediate formation of methanol. Gesser *et al.* (2) recently reviewed the controlled oxidation of CH_4 to CH_3OH emphasizing the free radical mechanistic aspects. The heterogeneous catalytic studies was reviewed by Foster (3) and Pitchai and Kleir (4). Although the literature indicated some potential catalysts (5) no commercial viable reaction system has been developed. Before embarking on a study of the catalytic conversion of CH_4 to CH_3OH we attempted to establish a base-line study by examining the homogeneous reaction (6,7,8,9) and here report a summary of the results with methane.

EXPERIMENTAL

The experiments were performed in a glass lined tubular reactor (0.36 cm ID, 3.3 mL heated volume). Reaction temperature was indicated by a steel sheathed thermocouple probe in the reaction zone.

Gases (2% N_2 in CH_4 and pure O_2) from the respective cylinders were thoroughly pre-mixed before entering into the reactor by passing them through a mixing cross filled with Teflon turnings. Nitrogen was deliberately introduced into the feed gas so as to act as an internal reference. The pressures at various points were monitored by calibrated pressure transducers. The reaction products were analyzed by gas chromatography with a thermal conductivity detector using an 8-port sampling valve and two columns -- 5A molecular sieve and a Porapak S column.

Using N_2 as an internal reference it was possible to measure the changes in the ratio $(\text{CH}_4/\text{N}_2)_{\text{in}}$ to $(\text{CH}_4/\text{N}_2)_{\text{out}}$ and so determine the conversion and material balances. Selectivity was calculated in terms of total carbon products. The water yield was invariably greater than that of the methanol. Formaldehyde was found in trace quantities and was determined colorimetrically (10).

Experiments were conducted by first adjusting the gas flows and, when stable, the temperature of the reactor was raised to the desired value. The on-line analysis was then performed over a period of several hours.

The residence time was usually about 2 minutes but varied from 0.2 to about 5 min with no obvious effects on the products.

RESULTS

The effect of temperature on CH_3OH conversion at different temperatures and pressures is shown in Figure 1. At higher O_2 concentrations the increase in temperature significantly increases the conversion. The possible CH_4 conversion is a maximum of twice, and a minimum of half, the O_2 consumed. Calculated conversion of greater than twice the O_2 consumed were due to errors in the CH_4/N_2 ratios

measured and the accompanying errors in the differences of two large numbers. Material balances were usually good (within 100 ±10%) for carbon but poor for oxygen.

The results in Figure 2 show the effect of temperature on the methanol selectivity at various O₂ concentrations. As the temperature is increased the selectivity passes through a maximum which is at lower temperatures for lower O₂ concentrations.

The methanol selectivity decreases as the O₂ concentration increases as shown in Figure 3.

The effect of pressure on the methanol selectivity was determined in another reactor (0.4 cm ID, 5.7 mL reactor volume). The results are given in Table 1 and clearly show that for a given oxygen concentration in the feed gas and, given reaction temperature, pressure had a positive influence on methanol selectivity; especially at above 50 atm. Thus, at an oxygen concentration of 5 to 6% in the feed gas and a reaction temperature of about 453°C, the methanol selectivity increased from 65% at 35 atm to 76% at 50 atm and at 65 atm it was 83%. A similar trend was observed at the other oxygen concentrations used in this study.

DISCUSSION

Much of the earlier work on partial oxidation of methane has been conducted in static reactors (11,12). Limited studies have been performed employing flow reactors at high pressures (13,14,15). Boomer *et al.* (16) showed that at a pressure of 180 atm, temperature of 475°C and 3.2% oxygen concentration in the feed gas, a maximum methanol selectivity of 74% could be obtained. The methane conversion at the above conditions was only 1.9%. Similar results were reported by Pichler and Reder (14), and Wiezevich and Frolich (15). Brockhaus and Franke (17) from their studies on the partial oxidation of methane under cool flame conditions were able to obtain a combined selectivity of methanol and formaldehyde of up to 91%. However, the conversion per pass was of the order of 2%. In comparison to all of the studies reported to this date on homogeneous gas phase oxidation of methane, our results seem to be the most promising in that a methanol selectivity of 83% at a conversion level of 8% per pass could be obtained.

The high methanol selectivities observed in our experiments can be explained by the type of the reactor used and the reaction conditions employed in the study. Several workers (18,19) have identified surface reactions such as oxidation, decomposition of oxygenated products and coke formation to be responsible for the decrease in methanol selectivity. Surface reactions were found to be important in metal reactors, packed reactors and also at low reaction pressures (20). In our study, probably the surface reactions were of less importance due to the use of a glass lined and/or high pressure where diffusion to reactor wall would not be significant.

The proposed mechanism for the partial oxidation of methane at high pressure (12) suggests that the reaction between the peroxide radical CH₃O₂ and methane resulting in the formation of methylhydroperoxide and methyl radicals may compete strongly with the decomposition of the peroxide radical. The methylhydroperoxide radical then decomposes into methoxy and hydroxy radicals and methanol is formed by a reaction between the methoxy radical and methane. Hence, higher pressures favour the methanol selectivity and our results as shown in Table 1 support this view. Although in the present work the maximum reaction pressure employed was 65 atm, earlier experiments (6,21) showed that an increase in pressure to 125 atm had lower methanol selectivity. Thus at an oxygen concentration of 5% in the feed gas the methanol selectivity was found to decrease from 81% at 50 atm to 25% at 125 atm. The maximum methanol selectivity may occur between 65 and 125 atm and this has yet to be established.

CONCLUSIONS

In this study we showed that methanol selectivities of 75 to over 80% at 8 to 10% conversion levels per pass could be obtained during the partial oxidation of methane in the tubular reactor operated at about 65 atm, 450°C and a residence time of about 4 min. The methanol selectivity was observed to depend significantly on

the oxygen concentration in the feed gas and reaction pressure. Oxygen concentrations less than 5% and reaction pressure higher than 50 atm were found to be conducive for higher methanol selectivity.

ACKNOWLEDGEMENT

The authors are grateful to Energy, Mines and Resources, CANMET of Canada for providing the financial support during the entire study.

REFERENCES

1. Edwards, J. H., Foster, N. R., Fuel Science & Technology Int'l 4, 365 (1986).
2. Gesser, H. D., Hunter, N. R., Prakash, C. B., Chemical Reviews, 85, 235 (1985).
3. Foster, N. R., Appl. Catal., 19, 1 (1985).
4. Pitchai, R., Klier, K., Catal. Rev. Sci. Eng., 28, 13 (1986).
5. Liu, H. F., Liu, R. S., Liew, K. Y., Johson, R. E., Lunsford, J. H., J. Am. Chem. Soc., 106, 4117 (1984).
6. Hunter, N. R., Gesser, H. D., Morton, L. A., and Prakash, C. B., Proceedings of the VI International Symposium on Alcohol Fuels Technology, Ottawa, May 21-25 (1984).
7. Hunter, N. R., Gesser, H. D., Morton, L. A., and Fung, D. P. C., Proceedings of the 35th Canadian Chemical Engineering Conference, Calgary, Oct. 6-9 (1985).
8. Gesser, H. D., Hunter, N. R., Morton, L. A., U.S. Patent No. 4,618,732, Issued Oct. 21, 1986.
9. Yarlagadda, P. S., Morton, L. A., Hunter, N. R., and Gesser, H. D., Fuel Science & Technology Int'l (in press).
10. Newitt, D. M., Haffner, A. E., Proc. Roy. Soc. London, A134, 591 (1932).
11. Lott, J. L., The selective oxidation of methane at high pressure, Ph.D. Thesis, University of Oklahoma (1965).
12. Newitt, D. M., Szego, P., Proc. Roy. Soc. London, A147, 555 (1934).
13. Pichler, H., Reder, R., Angewandte Chemie, 46, 161 (1933).
14. Wiezevich, P. J., Frolich, P. K., Ind. Eng. Chem., 26, 267 (1934).
15. Boomer, E. H., Can. J. Res., 15B, 375 (1937).
- 16a. Boomer, E. H., Thomas, V., Can. J. Res., 15B, 401 (1937).
- 16b. Boomer, E. H., Thomas, V., Can. J. Res., 15B, 414 (1937).
- 16c. Brockhaus, R. and Franck, H.-J., Deutsches Patentant 2,743,113 (1979).
17. Mahajan, S., Menzies, W. R., Albright, L. F., Ind. Eng. Chem. Process Des. Dev., 16, 271 (1977a).
- 18a. Mahajan, S., Nickolas, D. M., Sherwood, F., Menzies, W. R., Albright, L. F., Ind. Eng. Chem. Process Des. Dev., 16, 275 (1977b).
- 18b. Mahajan, S., Nickolas, D. M., Sherwood, F., Menzies, W. R., Albright, L. F., Ind. Eng. Chem. Process Des. Dev., 16, 275 (1977b).
19. Lott, J. L., Sliepcevic, C. M., Ind. Eng. Chem. Process Des. Dev., 6, 67 (1967).
20. Chou, T. C., Albright, L. F., Ind. Eng. Chem. Process Des. Dev., 17, 454 (1978).
21. Gesser, H. D., Hunter, N. R., Morton, L. A., Prakash, C. B., The Production of methanol by the controlled oxidation of methane at high pressures, Final Report submitted to Energy, Mines and Resources Canada (1984).

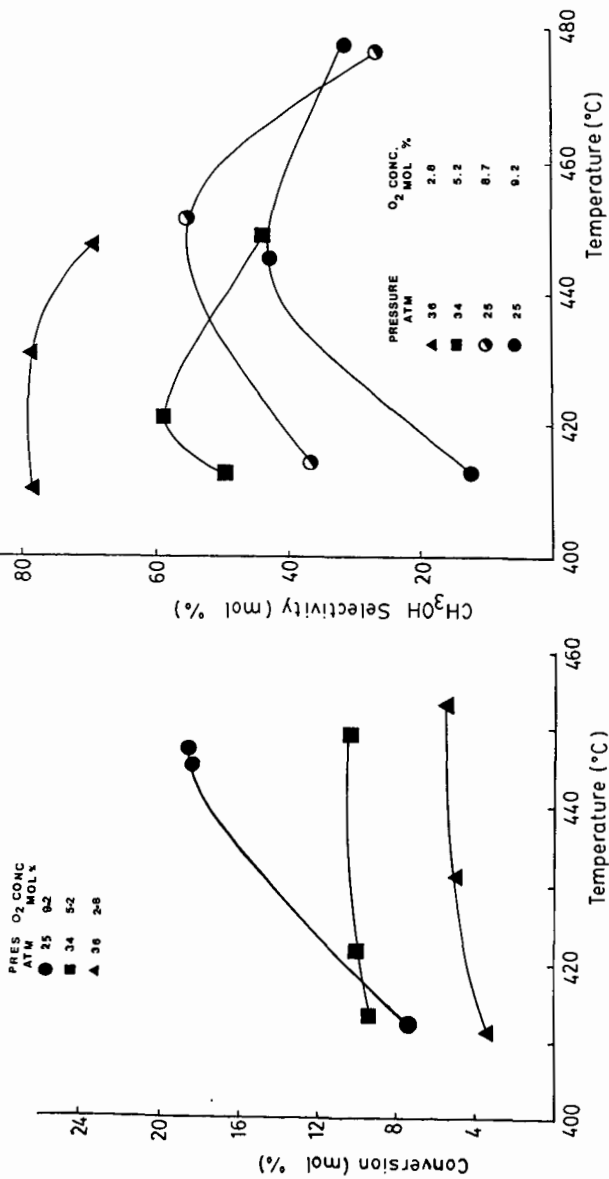


Figure 1. Effect of reaction temperature on conversion at different combinations of reaction pressure and oxygen concentrations in the feed gas.

Figure 2. Variation in methanol selectivity with reaction temperature.

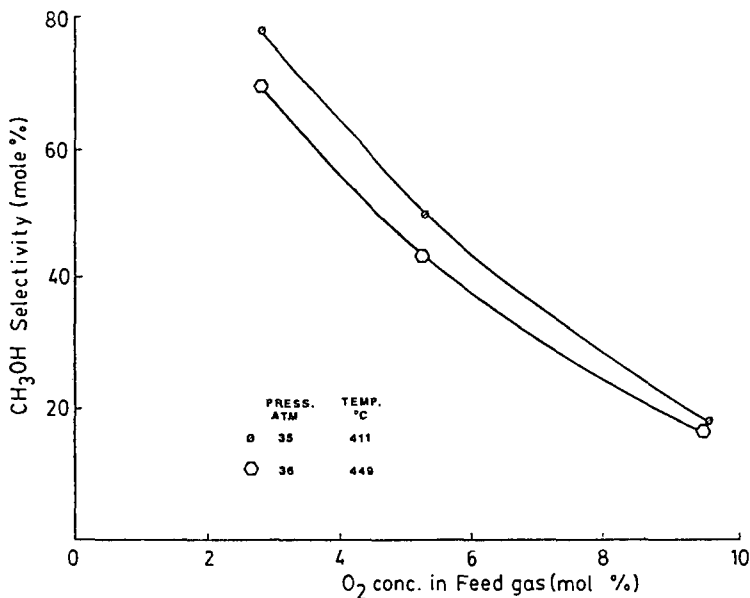


Figure 3. Effect of oxygen concentration in the feed gas on methanol selectivity.

Table I. The effect of varying reaction pressure on methanol selectivity at different oxygen concentrations in the feed gas.

Run #	Reaction Conditions			Residence Time min	Conversion mol%	Selectivity, mol%*			CH ₃ OH Yield mol%
	Temperature °C	Pressure atm	O ₂ Conc. mol%			CH ₃ OH	CO	CO ₂	
29	455	34.0	10.3	2.5	7.5	59.8	25.1	15.1	4.5
28	453	34.7	6.0	3.5	8.1	64.9	20.7	14.7	5.3
27	450	34.4	2.1	3.2	3.9	77.0	10.7	12.3	3.1
26	453	50.0	8.0	2.8	7.5	56.5	23.9	19.3	4.3
24	451	50.0	6.7	3.7	9.5	76.0	12.6	11.4	7.2
25	451	50.0	3.5	4.6	5.9	76.7	12.6	10.7	4.5
32	456	65.4	7.4	4.5	11.0	66.5	22.6	10.9	7.3
31+	456	65.3	5.1	4.1	8.0	83.0	10.7	6.4	6.6
33	468	65.6	2.6	3.7	5.3	81.5	9.6	8.9	4.3

*Average of at least 4 on-line analysis.

+Reducing the heated zone from 45 cm to 35 cm increased the CH₃OH selectivity to 84.5%.

Methane Polymerization Using a Hollow Cathode

Paul Meubus* and Gilles Jean**

*Université du Québec à Chicoutimi,
Qué. Canada G7H 2B1

**CANMET Laboratories, Ministry of Energy, Mines and Resources
Ottawa, Ontario, Canada K1A 0G1

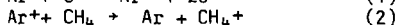
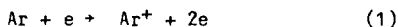
Introduction

The polymerization of methane, or other low-molecular weight hydrocarbons, in the presence of electrical discharges or in low temperature plasmas, has been the subject of a large number of reports in the literature (1-3). Common features are the operation under vacuum and the production of radicals diffusing towards the reactor wall with subsequent polymerization to a solid product. The gas phase is generally composed of hydrocarbons up to C₅. The polymerization of hydrocarbons can be initiated through the positive-ion molecule type reaction and the radical molecule type reaction (4). The hollow cathode is a medium of high interest for generating a large concentration of highly energetic electrons, leading to the possible formation of CH₄⁺ ions.

Preliminary results obtained in this lab (5-6) have shown that methane conversion can be effected using a hollow cathode as the source of polymer initiators. The present work investigates the effects on the process of the cathode metal used (Tungsten, Tantalum and a Tungsten-Platinum solid solution) as well as the influence on the yield of the gas used as a diluent (argon and helium).

Theory

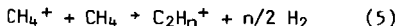
Within the hollow cathode, an atom or molecule is ionized following energy transfers resulting from atom - electron collisions or charge transfer (7). With mixtures of Ar-CH₄ and He-CH₄, the ionization step of methane takes place according to the reactions:



Also, argon metastables ³P₂ (11.54 eV) and ³P₀ (11.72 eV) can be generated:



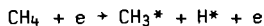
Similar reactions may occur with He* which presents a metastable level at 19.8 eV, this particle being then much more energetic than the argon metastables. The polymerization then proceeds following the equation:



the chain reaction yielding C_mH⁺_n. Termination of the process occurs when low velocity electrons are available:



The steps described are not unique and low velocity electrons can also lead to the formation of radicals, this likely occurring at the outlet of the cathode:



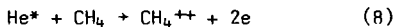
and the process continues through hydrogen abstraction.

Experimental

The reactor is shown in Figure 1. It consisted mainly of an arc discharge with a cylindrical hollow cathode 4 cm long and 0.2 cm thick. The cathode materials used were tungsten, a solid solution of tungsten and platinum and finally tantalum. The anode was made of stainless steel with a water-cooled tungsten discharge tip. The electrodes were located in a cooling chamber where the polymer obtained was collected on the water-cooled walls. A Varian 1015SL quadrupole mass spectrograph was used for the effluent gas analysis. High purity argon and chemical pure (99.9% purity) methane were used in mixtures up to 25% methane by volume. Depending on the experiment, the electrode gap was adjusted between 1.5 and 4.0 mm. The cathode furnace was adjusted to 2400°K while the arc discharge was started and the required methane flow added to the main argon stream. Further adjustments were then made in order to operate at the pre-determined conditions. The duration of an experiment was typically 10 minutes and the initial adjustments lasted about 30 seconds. At the end of the run, the polymer deposited on the cooled wall of the reactor was collected, together with the carbon appearing on the electrodes. They were weighed to the nearest ±0.1 mg.

Results and Discussion

The main product resulting from the conversion of methane using the hollow cathode is a solid polymer. Figure 2 illustrates the relationship between polymer yield, defined as weight of polymer/weight of methane fed, and E/P (E = electric field between electrodes, V-cm⁻¹; P = pressure, Torr). This yield is a function of the average electron energy. The maximum polymer yield is about 50% higher in helium than in argon, the corresponding E/P value for helium being about twice the one required for argon. The higher polymer yields obtained with helium are possibly related to a higher rate of formation of CH₄⁺. For instance:



taking into account the presence of the highly energetic He⁺ (ionization voltage 24.6V) and He* (19.8V).

When Helium is used as diluent higher CH₄ concentrations do not seem to significantly affect the maximum polymer yield (Figure 3). In argon, increases in methane concentration lead to decreasing polymer yields as shown in Figure 4 curve 2 B. Higher polymer yields can be obtained at high concentration by increasing the cathode voltage. At high methane concentration only methane, acetylene and ethylene were found in the gas phase which is probably the result of propagation reaction steps having been interrupted by termination reactions with slow electrons or radicals recombination.

Another interesting feature observed in the case of CH_4/He mixtures is the complete absence of carbon deposits. The hydrocarbon species present are characterized by higher diffusivities in He than in Ar (Ar). This may be responsible for higher deposition rates of the hydrocarbon species present in the gas phase on the reactor wall. It could also, at least partly, explain the decreasing effect of competitive reactions leading to the formation of carbon when argon is used as a diluent gas.

Besides tungsten (work function $Q_w = 4.6$ eV), tantalum ($Q_{Ta} = 4.1$ eV) and a tungsten-platinum solid solution were used to study the influence of cathode material on polymer yield. The work function of the W-Pt cathode was evaluated to be 6.5 eV. This result compares rather closely with the 6.3 eV obtained for the Pt cathode.

These cathodes were tested with Ar+ CH_4 mixtures. Figure 4 illustrates the comparative behaviour of W-Pt and W cathodes. For 10% CH_4 mixtures a high yield is obtained for the W-Pt cathode, the yield decreasing with increasing electrons energy (curve 1A). For the 25% CH_4 mixture the yield increases with increasing electron energy for both the W-Pt and the W cathodes (Curve 1B and 2B). Tungsten cathodes operating at the same conditions show significantly lower conversions, although the behaviour of yield vs E/P is the same (curves 2A and 2B).

The current density for the W-Pt cathode is estimated to be 10% that obtained with the W cathode. The drift velocity being similar in both cases, one would expect a lower electron concentration (of the same energy) for W-Pt cathodes. As a consequence, lower rates of formation of polymerization promoters and lower polymer yields should be obtained with the W-Pt cathode compared to the W cathode. To explain the higher yields observed the assumption is then made that the W-Pt cathode surface does play a catalytic role whose contribution increases as electron energy decreases (6). Figure 5 shows the relative behaviour of tantalum and tungsten cathodes. Although the thermoemissive characters of Ta and W are rather similar, tantalum does show only an increase in yield with a corresponding increase of electron energy (curve 1C, Figure 6). It is possible that catalytic effects are absent in this case, in opposition to the tungsten behaviour (curve 2A).

Conclusion

Using helium instead of argon in the polymerization of methane, by means of a hollow cathode, increases the rate of polymerization and suppresses carbon formation. These conclusions only apply to low methane concentrations (10%). Tungsten (1), tantalum (2) and a solid solution tungsten-platinum (3) have been used for making hollow cathodes. Besides being the site of highly energetic collisional processes, cathodes 1 and 3 seem to play a catalytic role in the formation of polymerization promoters. In this respect, cathode 3 shows high yields of polymer formation.

Acknowledgement

The authors are indebted to the Federal Ministry of Supply and Services and to the Federal Ministry of Energy, Mines and Resources Canada for financial support under contract no. 375123440-5-9233.

References

1. A.M. Millard, Techniques and Applications of Plasma Chemistry, J.R. Hollahan and A.I. Bell, eds. Wiley, New York (1974).
2. M. Shen, Plasma Chemistry of Polymers, Marcel Dekker, New York (1976).
3. H. Yasuda, Thin Film Processes, J.L. Vossen and W. Kern, eds., Academic Press, New York (1978).
4. C.E. Melton, J. Chem. Phys., 33, 647 (1960).
5. P. Meubus, Conversion du Méthane en Essence Automobile par Réactions en Cathode Creuse. Report to Can. Feder. Ministry of Energy, Mines and Resources (1986).
6. P. Meubus, Polymerization of Methane in a Hollow Cathode Discharge, 35th Canadian Chemical Engineering Conference, Calgary, Canada, October 6-9 (1985). Paper 7-63.
7. J.B. Hasted, Physics of Atomic Collisions, Butterworth, London (1964).
8. R.J. Jensen, A.I. Bell and D.S. Song, Plasma Chemistry and Plasma Processing, Vol. 3, 2, 1983.

Figure 1 Outside view of reactor

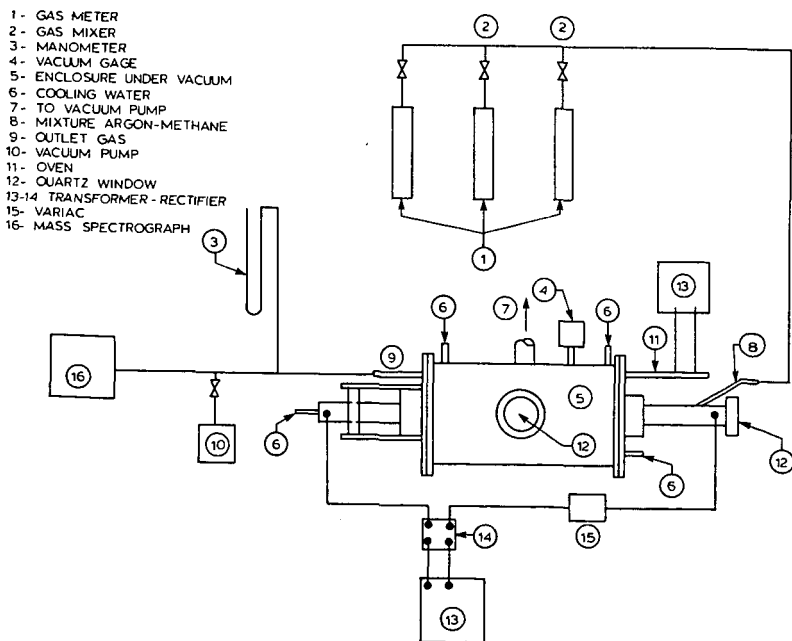


Figure 2. EFFECT OF GAS DILUENT

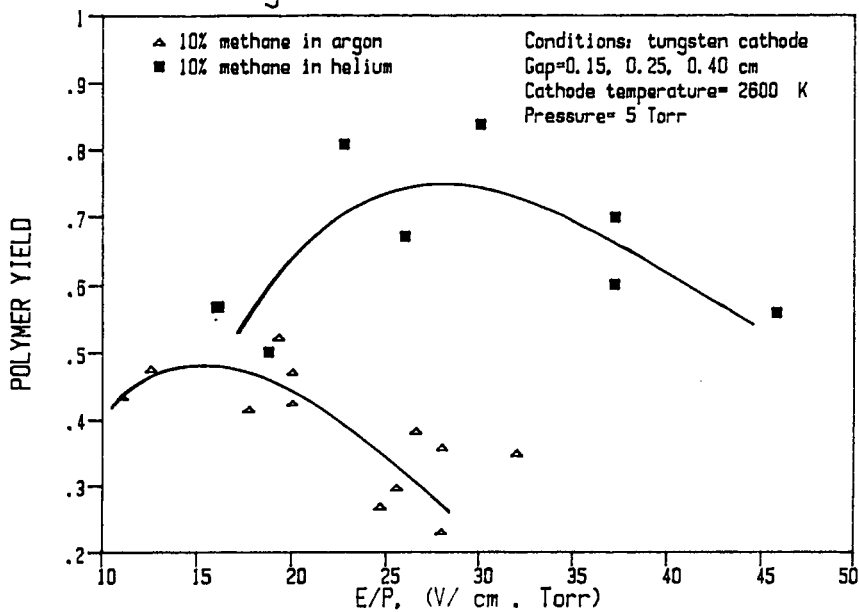


Figure 3. EFFECT OF METHANE CONCENTRATION

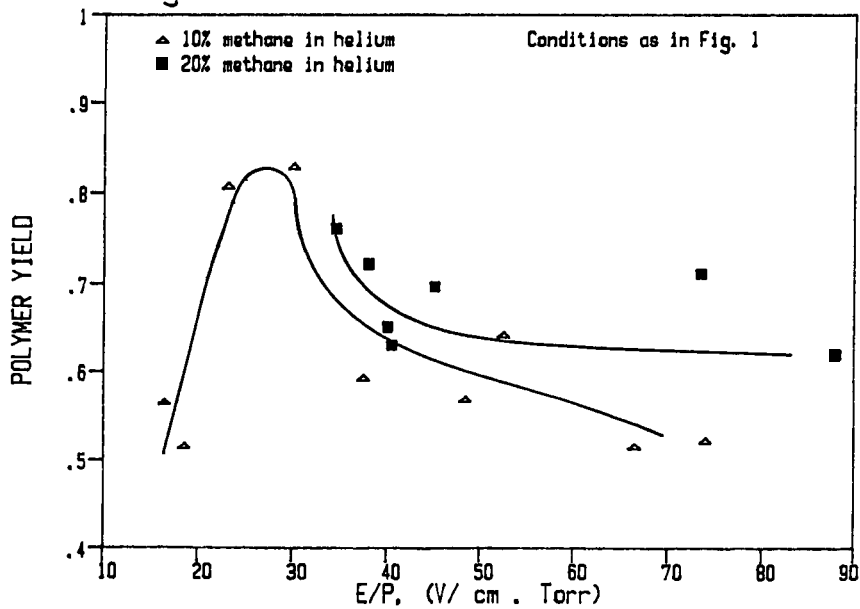


Figure 4. EFFECT OF CATHODE MATERIAL

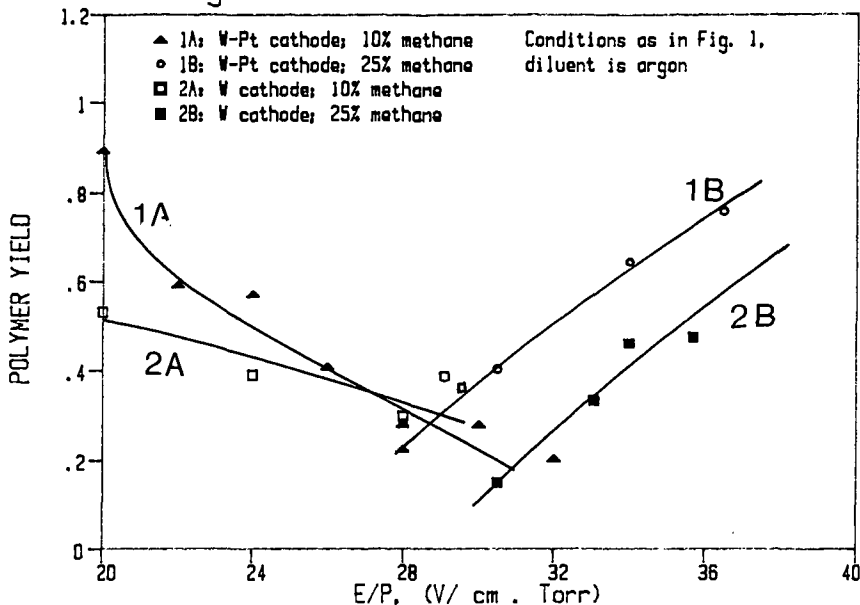
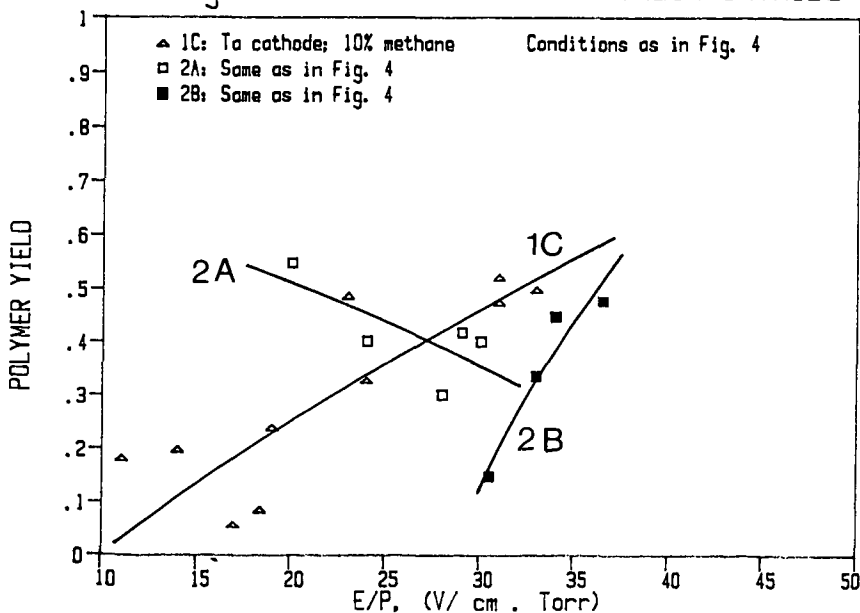


Figure 5. BEHAVIOR OF TANTALUM CATHODE



Methane Partial Oxidation in Alternating Electric Fields

R. G. Mallinson and C. M. Sliepcevich

School of Chemical Engineering and Materials Science
University of Oklahoma
Norman, Oklahoma 73019

S. Rusek

Technical Center
Owens-Coming Fiberglas
Granville, Ohio 43023

ABSTRACT

In this work, methane and oxygen mixtures have been oxidized to form methanol and smaller amounts of formaldehyde, methyl formate, formic acid and ethanol. Substantial amounts of water are also produced, as well as a small amount of ethane. The oxidation takes place at ambient conditions of temperature and pressure in an alternating electric field which is generated between cylindrical plates with a gap of 0.060 inches. Conversions were linearly dependent on the RMS voltage in experiments using up to 10 kV RMS. Among square, triangular, and sinusoidal wave forms, only small differences in performance were observed over the range of frequencies studied, from 25 to 200 Hertz. The effects of oxygen concentration, space time, frequency, and field plate area have also been examined on a limited basis. The power consumption to the power supply has been measured to determine the efficiency of this system, in which substantial heat is released. The yield of methanol is from seven to nine percent of the methane converted in which methane conversions of five to ten percent are obtained when an oxygen limited feed is used. Substantial amounts of the methane converted appear as carbon monoxide and carbon dioxide, both of which are somewhat inhibited by operation with the oxygen limited feed, although product inhibition during recycle experiments was not observed.

INTRODUCTION

There is currently a great deal of interest in the production of organic oxygenates via partial oxidation. Of particular interest is the conversion of methane to liquid fuels such as methanol, as well as the synthesis of other single and multiple carbon products such as formaldehyde, ethanol and acetic acid. Most current research involves the use of heterogeneous catalysts (1), although there has been some effort in examining thermal routes (2). It is only in the relatively old literature that the partial oxidation of methane in the presence of electric fields appears.

EXPERIMENTAL

The experimental reaction system was operated in three different configurations, however most of the results of this paper were obtained in the single pass mode. Figure 1 illustrates this configuration. Oxygen and methane are fed through individual rotameters and mixed and then flow to the reacto inlet. The reactor is the reaction vessel from an OREC model 03V5-0 ozone generator. The outer shell is a stainless steel cylinder with an outlet at the bottom. This shell serves as one electrode. The inside diameter of this outer shell is 77 millimeters. Within this shell, a glass tube is fitted which has a sealed bottom and the inner electrode which covers the inside surface of the glass tube. The gap between the outer wall of the glass tube and the inner wall of the shell is nominally 1.5 mm. Thus the

"active" reactor volume is in the shape of an annulus with an axial length of 332 mm. No analysis of the mixing characteristics was conducted, but it may be expected that there is some degree of backmixing. The volume of the reactor, between the electrodes, is about 118 cc, and the electrode area about 787 square centimeters. (The last experiment was conducted with one half of this plate area.) The outer shell has a water jacket made of PVC for control of the temperature by use of a water recirculation system or tap water.

After the gases have passed through the reactor, they pass through a dry ice/acetone trap to remove any condensable products. Following this, a small portion of the stream is diverted to a paramagnetic oxygen analyzer and, for later experiments, to a Carle gas chromatograph for analysis of the gaseous reactants and products. The thermal responses for all species detected were calibrated with known standards.

Power to the electrodes is provided by an Elgar AC power supply and a Wavetek function generator is used to generate the triangular wave used in the experiments discussed here. An oscilloscope is used to monitor the waveform, voltage level and frequency. A digital voltmeter is also used to monitor the RMS voltage.

A few experiments were run in a recycle configuration, illustrated in Figure 2. Mass flow controllers were used to add methane and oxygen to the system in a make-up gas stream. A Cole-Parmer diaphragm pump was used to recirculate the gas stream, with a bypass valve to maintain pressures slightly above atmospheric in all parts of the system.

RESULTS AND DISCUSSION

Initial runs were conducted at conditions previously established as optimal for a standard set of conditions (3). The feed flow rate was 566 cc/min at 71 ° F with a composition of 24.4 volume percent oxygen and 75.7 percent methane at a pressure of 12 inches of water. The reactor was maintained at 155 ° F. The electric field was maintained at 8 kV RMS at a frequency of 200 Hz using a triangular waveform. Under the standard conditions, the conversion of methane was about 15 percent and that of oxygen about 24 percent. Replicate experiments showed that the conversions of methane and oxygen varied ± 15 percent and ± 10 percent, respectively. The fractional yields of the primary liquid products under these conditions, water and methanol, were about .07 for methanol and .33 for water. The fractional yield is defined as the moles of a product produced per mole of methane reacted. This is used for water even though it is not a carbon based product. Thus about 7 percent of the methane converted formed methanol. Although methanol was the primary product, smaller amounts of other one and two carbon oxygenates were also formed. These products include formaldehyde, ethanol, methyl formate and formic acid. Qualitative GC/MS data showed the presence of numerous other compounds in minute quantities.

Run 4 was conducted to determine the variation on the oxygen conversion with changes in the field voltage. The oxygen concentration in the exit stream was used as an indicator of reactivity before more detailed analyses were made with later runs. In this experiment, the field was increased in increments from zero volts and allowed to equilibrate for several minutes. No decrease in the exit gas oxygen concentration was observed below 5 kV. At and above 5 kV the steady state oxygen concentration in the exit gas stream decreased linearly with increasing voltage. The system could attain a maximum RMS voltage of about 8kV at a frequency of 200 Hz. At 8 kV, the exit oxygen concentration was about 19.5 percent, or a conversion of 22 percent. A later run, run 25, was made to assess the effect of the frequency on the conversion and this, too, was found to be linear with decreased conversions at lower frequencies. In this run, the line power to the power supply was monitored and at a frequency of 50 Hz, the power consumed was approximately 30 percent of that at 200 Hz. The power used at 200 Hz was 350 Watts. There did appear to be some selectivity enhancement under these

conditions, as the methanol produced had decreased to about 43 percent of its amount at 200 Hz. However, the decrease in conversion would have a significant influence on the optimal frequency for operation.

Because significant amounts of carbon dioxide and water were produced, as well as the desired organic oxygenates, it was desirable to see if these might be inhibited by introduction of these species to the inlet stream of the reactor. Depending on the kinetics, it might be expected that significant quantities of these two species might drive the equilibrium in a favorable direction. In run 19, the inlet mole fraction of oxygen was reduced to .188 and a mole fraction of carbon dioxide of .085 was added, with the balance methane and the total inlet flow rate 485 cc/min. No differences could be detected in the results compared to runs at standard conditions, thus indicating that no equilibrium constraint appears to be limiting for carbon dioxide.

Run 20 was similar to run 19 except that an inlet mole fraction of water of .021 was used instead of the carbon dioxide. The water was added by saturating the inlet gas stream through a bubbler assembly. As with run 19, no remarkable results were observed here.

Although the reactor was being heated to 155 ° F, no work had previously been done to determine the effect of temperature on the reactions. Run 14 was made at ambient temperature, and it was observed that no effects due to the lower temperature were present. All runs subsequent to run 14 were, therefore, made at ambient temperature. It was noted that, in fact, significant quantities of heat were generated and a stream of cooling water was passed through the reactor water jacket to maintain ambient conditions. Measurements of the temperature rise of the cooling water through the jacket and its flow rate were made on several occasions. Although the accuracy may be considered poor, it appears that a significant fraction of the input power to the system may be dissipated as heat.

Because of the complete oxidation of a fraction of the methane to carbon dioxide, several experiments at lower increments of inlet oxygen concentration were made. The lowest concentration examined was about 1 percent oxygen. In run 23, the inlet mole fraction of oxygen was .012. The power required to maintain the 8 kV field increased somewhat, to 377 Watts. The conversion of the methane decreased substantially to .059, and the small amount of oxygen was about 49 percent converted. The yield of methanol remained near the standard value, about .073. The yield of water was substantially reduced, to .125, as might be expected with significantly less oxygen available. Interestingly, ethane now became a significant product from the methane. This would certainly indicate active methyl species participating in the reaction sequence. Another reactor configuration was used for one run, in which only the oxygen was passed through the reactor. This stream was then immediately mixed with methane to determine whether only active oxygen species, primarily ozone, might be the primary locus of the reactions. No reaction at all was observed in this case, and the literature on ozone chemistry agrees with the inability of ozone to significantly attack methane. Clearly the observed reactions indicate direct participation of active methane species.

A last standard experiment was made with one half of the inner electrode plate area. The results indicated that, while conversions tracked the decrease in the area, the power did not decrease by 50 percent. Thus, the inverse extrapolation for scale up would be that a 100 percent increase in the plate area, suitably configured, would result in a doubling of the quantities converted, but at less than a doubling of the power requirement, which is a favorable conclusion. The quantity of power used as "over-head" in the power supply was not determined. Attempts to measure the actual power used in the reactor field were unsuccessful, but it has already been mentioned that substantial heat was generated.

In the recycle configuration, two experiments were made. The only difference between them was the recycle flow rate. The carbon dioxide absorber shown in Figure 2, was not used for these runs. For run 29, the recycle flow rate, including make up gas, was 2.1 l/min, and for run 30, 1.0 l/min was used. The composition of gas entering the reactor was .005 mole fraction oxygen, once the reaction

had been underway for a short time. A material balance on the carbon and oxygen was made at the end of each run. The condensed products could only be removed after the system was shut down. The carbon balance was able to account for 73 percent of the carbon in the methane cumulatively provided to the system, initially and during the run. At the end of a ninety minute run, for run 30, about 112 millimoles of carbon, as methane, had been fed to the system, of which about 55 remained in the system or was lost in the GC bleed stream. About 2.6 millimoles of carbon went to produce ethane, about 4.7 as carbon dioxide and 5 as carbon monoxide. 15 millimoles of methanol were produced, but other organic compounds were not quantified and could be approximately 5 more millimoles. Thus, in this initial system configuration, approximately 13 to 17 percent of the methane used was converted to useful products. It may be that better material balances will enhance that figure to some extent.

On line GC analysis of the gases showed that ethane increased to a maximum of 1.2 and 1.4 millimoles in the system for the two runs, with the lower recycle rate having the higher maximum. Both maxima occurred about 40 minutes into the run, after which the concentrations both decreased by about 0.2 millimoles at the end of the 90 minute runs. Ethane, therefore appears to exhibit an equilibrium behavior. The carbon monoxide produced showed an induction period for the first 20 minutes, then continued increasing until the end of the run. Both experiments had virtually the same amount of carbon monoxide. Carbon dioxide increased linearly with time after also showing some induction during the first 20 minutes of the runs. However, the carbon dioxide produced at the higher recycle rate was significantly higher. At the end of the runs, the 2.1 l/min recycle rate had produced 6 millimoles of carbon dioxide, while the lower recycle rate had produced 4.7. One might think that the shorter contact time of the higher recycle rate would serve to minimize larger extents of oxidation.

The oxygen balance was able to account for 87 percent of the oxygen fed to the system. It might be noted that the oxygen conversion per pass was essentially 100 percent, and that higher inlet concentrations might alter the results obtained. Of the 40 millimoles of oxygen provided during the run, 5 appeared as carbon monoxide, 9.4 as carbon dioxide and 12 as water. Methanol accounted for 7.5 millimoles of the total.

The most significant result of the recycle experiments was that the percent methanol in the liquid product increased from one percent in the single pass runs to 12 percent for the recycle runs. Water concentration also increased, however.

Lastly, mention should be made that a number of other single pass experiments were conducted, both in search of other interesting reactions and in attempting to elucidate the reaction pathways of the methane-oxygen system. These runs were made at the standard conditions except that the species of the feed mixtures were altered. Mixtures examined were: carbon dioxide-methane, carbon monoxide-methane, hydrogen-nitrogen and carbon monoxide-hydrogen. Except for a trace amount of material produced from the carbon dioxide-methane mixture, no reactions were detected.

SUMMARY

The results from a number of scoping runs examining a number of variables have been presented for the oxidation of methane in an alternating electric field. Several features of these results point the way to further needed experiments to determine the possibilities for production of light organic oxygenates from this process. Fundamental studies to determine the mechanistic paths would also be useful to help focus further research on the optimal conditions for maximizing the yields of desirable products and for determining the economic potential of the process.

ACKNOWLEDGEMENTS

This work was funded by Owens-Corning Fiberglas. We wish to thank John Olinger, Jim Wintgens and Dick Fowler for helpful discussions. Also, Jim Wintgens was involved in the

developmental work which led to this research.

REFERENCES

- (1) Pitchai, R. and K. Klier; *Catal. Rev.-Sci. Eng.*, **28**, 13 (1986).
- (2) Lockett, G. A. and B. Mile; *Combustion and Flame*, **26**, 299 (1976).
- (3) Rusek, S. and J. Wintgens, unpublished results (1985).

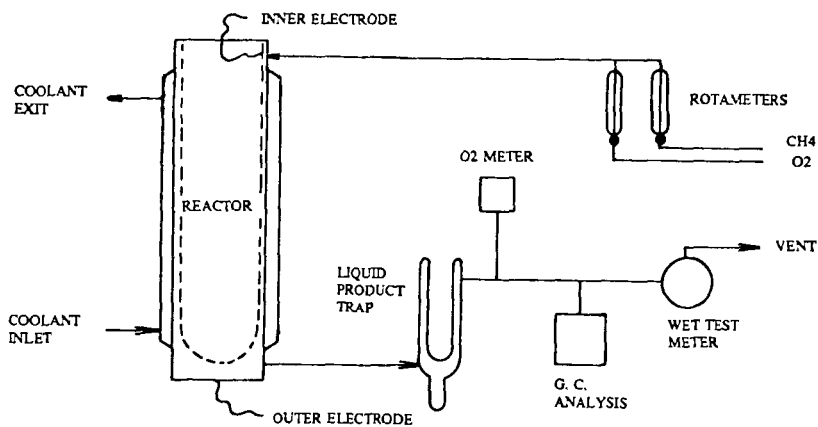


Figure 1. Single pass reactor system.

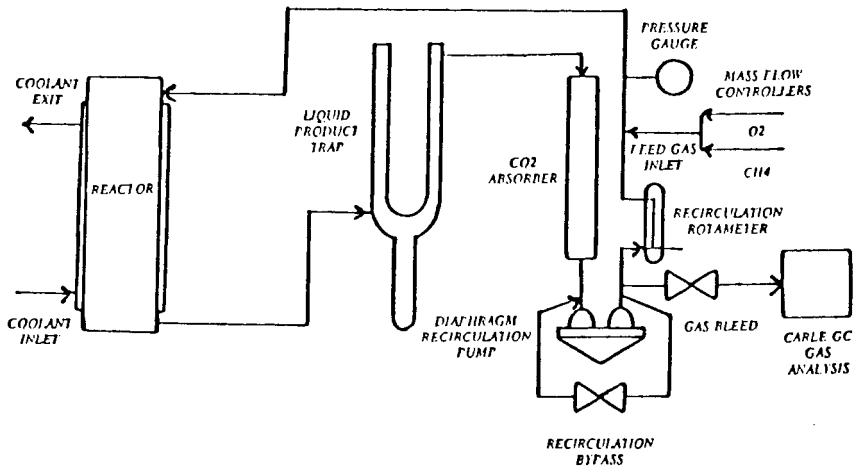


Figure 2. Recycle Reactor System.

NICKEL SITE OF METHANE CATALYSIS IN THE METHYL REDUCTASE ENZYME

J. A. Shelnut, A. K. Shiemke,* R. A. Scott*

Sandia National Laboratories, Albuquerque, NM 87185
University of Illinois, Urbana, IL 61801

Introduction

Methyl reductase is the enzyme of methanogenic bacteria that catalyzes the two-electron reduction of the methyl group of 2-(methylthio)ethanesulfonic acid (methyl-S-CoM) to methane and HS-CoM (1,2). The methyl group of methyl-S-CoM ultimately comes from the six-electron reduction of CO₂ by hydrogen, which also provides the reducing equivalents needed by methyl reductase. The nature of the catalytic site of methyl reductase is of current interest from the point of view of developing biomimetic C₁ chemistries directed toward methane synthesis and activation. In particular, Sandia is using molecular graphics and energy optimization techniques to design macromolecular catalysts that mimic the structure of sites of proteins that carry out C₁ chemistry. The goal is to produce catalysts whose function is the oxidation of low molecular weight hydrocarbon gases to generate liquid fuels or, alternatively, the reduction of abundant inorganic resources such as CO₂ to generate gaseous fuels. Unfortunately, the catalytic sites of many of the enzymes of interest, e. g. methyl reductase and methane monooxygenase, have not been characterized by X-ray crystallography and other structural techniques.

With the goal of learning more about the structure of one of these naturally occurring sites of C₁ chemistry, we have obtained the first resonance Raman spectra of the nickel-macrocycle, called F₄₃₀ (1 in Figure 1), at the site of catalysis in methyl reductase (3). To help us structurally interpret the Raman spectra of the enzyme we have also obtained Raman spectra of solutions of the major forms of F₄₃₀ (salt-extracted and cytosol-free) at room temperature and at 77 °K and also, under similar solution conditions, spectra of a nickel-corphinoid derivative (2 in Figure 1) that is related to F₄₃₀ (3-5). By analogy with the spectra of the model nickel-corphinoid 2, the F₄₃₀ Raman spectra characterize the coordination geometry of the nickel(II) ion in F₄₃₀ complexes in coordinating and non-coordinating solvents. In addition, the spectra give some information concerning macrocycle ruffling in the solution complexes. Although some conclusions about the F₄₃₀ site in methyl reductase can be made, the structure of F₄₃₀ in the protein environment is uniquely different from F₄₃₀ and the F₄₃₀ model compound in the solutions we have investigated.

Materials and Methods

Methyl reductase was prepared and purified as described previously (6). F₄₃₀ was isolated in two forms. Free F₄₃₀ was isolated from the cytosol by methods described before (7); F₄₃₀ was also extracted from the holoenzyme using a lithium-bromide procedure (6). The structure 1 of salt-extracted F₄₃₀ has been determined (8) and is shown in Figure 1. A nickel-corphinoid derivative related to F₄₃₀ and shown in 2 of Figure 1 was kindly provided by A. Eschenmoser, A. Pfaltz, and A. Fässler (9).

Samples of each chromophore (2-10x10⁻⁵ M) in aqueous solution buffered with 10 mM phosphate at pH 7 were used for obtaining resonance Raman spectra. Spectra of liquid solutions were obtained using a cylindrical cell partitioned into two compartments. The spectra of two samples were obtained simultaneously by rotating the cell at 100 Hz so that the two sample solutions were alternately probed by the laser radiation. The Raman difference instrumentation used for

detection and separation of the spectra of the two samples has been described previously (10). Peak positions were obtained from the fast-Fourier-transform smoothed spectra. For spectra run simultaneously the accuracy when comparing the frequency of the same Raman line in the two spectra is about $\pm 0.3 \text{ cm}^{-1}$. Occasionally, the solution of F_{430} or the corphinoid derivative was in one side of the cell and the reference side contained only the neat solvent. Subtraction of the solvent Raman lines could then be accurately accomplished leaving the spectrum of only the solute.

Raman spectra at 77°K were not obtained in the Raman difference mode, but separately using an EPR dewar with a transparent tail (Wilmad). The sample was contained in a 4-mm NMR tube and was frozen by plunging the tube into liquid N_2 . Reproducibility in the frequency of lines in these spectra are about 1 cm^{-1} .

Signal averaged Raman spectra were obtained using the 441.6-nm line of a HeCd laser (Omnichrome) or the 413.6-nm line of a krypton ion laser (Coherent). The spectral resolution was 4 cm^{-1} . Raman difference spectra were obtained using standard 90° scattering geometry; for spectra of frozen solutions a backscattering geometry was used. Absorption spectra as well as individual scans of the Raman spectrum were used to monitor sample integrity. No decomposition of F_{430} or the nickel-corphinoid model was observed.

Results

F_{430} and the model nickel-corphinoid complexes have an absorption band in the 410-440-nm region of the visible spectrum (9,11). Therefore, excitation of the Raman spectrum using 441.6-nm or 413.1-nm laser light is near the visible absorption band and, consequently, resonance enhancement of the Raman scattering occurs. In the case of the enzyme, resonance enhancement of the chromophore's spectrum permits us to selectively probe the macrocyclic cofactor without interference from the Raman spectrum of the protein matrix. Structural details of the F_{430} site in the protein can then be inferred from differences between the spectrum of protein-bound F_{430} and the spectra of F_{430} complexes in various solution environments. The spectra of all of the complexes are somewhat similar regardless of the position of the laser wavelength relative to the absorption band maximum of the particular complex. In fact, the frequencies and intensities of the lines are so similar that the corresponding lines in each of the spectra can easily be identified as can be seen in Figures 2-4. The Figures show typical spectra of salt-extracted F_{430} , cytosol-free F_{430} , and methyl reductase.

Figure 2 shows the Raman spectrum of LiBr-extracted F_{430} at room temperature and at 77°K . Two forms are present at room temperature. Form A has Raman lines at 1293, 1380, 1534, and (from other Raman data not shown) 1625 cm^{-1} ; the second form B has lines at higher frequencies—1312, 1382, 1555, and 1629 cm^{-1} . At low temperature form A disappears and only B remains.

Free F_{430} at room temperature is predominantly a single form with Raman lines at 1293, 1387, 1529, and 1623 cm^{-1} (Figure 3). The frequencies are similar but distinct from the corresponding lines of the A form of salt-extracted F_{430} . There is also some evidence of a small fraction of a form with lines near those of the B form in the weak shoulders of the high frequency lines. At low temperature this form is more abundant as evidenced by the appearance of lines at 1311, 1378, 1546, and 1616 cm^{-1} that are barely noticeable in the room temperature spectrum. There is also evidence for a second form at low temperature in the lines at 1292 and 1628 cm^{-1} . It is clear that this form is not the same as the one present at room temperature because the 1529-cm^{-1} line is not present or else is shifted to near 1546 cm^{-1} .

The Raman spectrum of methyl reductase at room temperature is markedly different from both the spectrum of salt-extracted F_{430} and free F_{430} . (Compare the spectra in Figure 4 with the corresponding spectra in Figures 2 and 3.) First, the Raman lines are clearly much narrower than for the solution F_{430} complexes. Second, frequencies of the two strong lines at 1575 and 1653 cm^{-1} are much higher than the corresponding lines of the F_{430} species. In contrast, the lines in the 1280-1400- cm^{-1} region of the methyl-reductase spectrum have frequencies comparable to F_{430} .

Differences between room temperature and 77-°K spectra of methyl reductase are much smaller than observed for F_{430} in solution. Increases in the intensity of the lines at 1312, 1553, and 1632 cm^{-1} indicate an enhanced fraction of a form of F_{430} with frequencies closest to those of salt-extracted F_{430} at 77 °K.

Discussion

Raman spectra of the F_{430} forms and the F_{430} model compound 2 are similar. For example, the nickel-corphinoid bis-methanol complex has several weak lines in the 1280-1400- cm^{-1} region and two strong lines at 1556 and 1627 cm^{-1} (4). Thus, the frequency of the lines and the intensities are similar for F_{430} and the model compound. The spectral similarities indicate that the nickel corphinoid 2 is generally a good structural model for F_{430} forms.

In previous work it was noted that the two strong highest frequency lines shift systematically with increasing coordination number (4). For example, the separation between the two lines decreases from 93 cm^{-1} for the 4-coordinate species (in CH_2Cl_2) to 84 cm^{-1} for a 5-coordinate NCS^- complex (in CH_2Cl_2) and to 71 cm^{-1} for the 6-coordinate MeOH complex. In fact, for a variety of solvents that axially ligate, the 6-coordinate separation is found to be 71±3 cm^{-1} (5). Ruffling of the corphinato macrocycle may also influence the separation (vide infra).

Salt-extracted F_{430} . Assuming that the separation of the two strong lines is indicative of coordination number for F_{430} as well as the model, we predict that aqueous salt-extracted F_{430} is a mixture of a dominate 6-coordinate complex referred to above as species B (with a separation of 1629 - 1556 = 73 cm^{-1}) and a minor 4-coordinate species A (with a separation of 1625 - 1534 = 91 cm^{-1}). Indeed, the separation varies from 62-75 cm^{-1} for F_{430} 6-coordinate complexes in other coordinating solvents (5). The existence of a mixture of a 6-coordinate high-spin species and a 4-coordinate S=0 species is supported by the intermediate value found for the magnetic moment (2.0 μ_B for F_{430} versus ~2.8 μ_B predicted for a pure S=1 species) (12).

The axial ligands are probably H_2O molecules rather than some component left bound to F_{430} after extraction from the protein. Water is a weak ligand which would account for the equilibrium mixture at room temperature. At 77 °K the equilibrium shifts overwhelmingly toward the bis-aquo F_{430} complex.

Cytosol-free F_{430} . Water appears to be a poorer ligand for free F_{430} than for the salt-extracted form, since at room temperature aqueous free F_{430} is almost entirely a 4-coordinate form. This conclusion is based on an observed separation of the strong high frequency lines of 94 cm^{-1} —a value close to the separation for the 4-coordinate model compound 2. By comparison, in strongly coordinating solvents and in the presence of CN^- , free F_{430} converts to a 6-coordinate form with a separation of 63-77 cm^{-1} (5).

At 77 °K free F_{430} appears to be a mixture of two forms with lines at 1616 and 1628 cm^{-1} . The separations of the 1616- and 1628- cm^{-1} lines from the 1546- cm^{-1} line are 70 and 82 cm^{-1} for the two forms. EXAFS and XAS measurements at 4 °K are consistent with free F_{430} (the same as heat-extracted F_{430}) existing as a mixture of predominantly a 4-coordinate, ruffled species with short Ni-N bonds (1.9 Å) and a minor 6-coordinate, planar species with longer Ni-N bonds (2.1 Å) (13). The Raman data is in agreement with this result. The species with the 70- cm^{-1} separation is probably the coordinated species and the 82- cm^{-1} separation species would then be the more abundant 4-coordinate, ruffled species. A 5-coordinate complex is unlikely for a nickel corphinate in a coordinating solvent where two axial ligands would be readily available and formation of the 6-coordinate complex would be favored. Alternatively, the two species could be different ruffled species, for example, the two species obtained by a 90 ° rotation of the saddle structure resulting from S_4 ruffling and inversion of the half chair conformation of the hydroppyrrrolic rings (12,15).

Comparison of the F_{430} forms. Eschenmoser and coworkers have suggested that the sole difference between free and salt-extracted forms of F_{430} is a di-epimerization at positions 12 and 13 in which the hydrogen and carboxylic acid at each position exchange places (12). The structural change also occurs upon heating salt-extracted F_{430} or upon heat-extraction of F_{430} from methyl reductase. The 12,13-diepimer of salt-extracted F_{430} results in a corphinate structure that can undergo S_4 ruffling more readily than F_{430} for steric reasons. Ruffling affects axial ligation because it allows the central core of the macrocycle to contract about the nickel ion. Thus, salt-extracted F_{430} is more coordinatively unsaturated at the nickel ion as a result of its larger core size, and, therefore, has a higher affinity for axial ligands than free F_{430} which can easily ruffle.

The Raman results are in agreement with this structural interpretation. At room temperature salt-extracted F_{430} is mostly the 6-coordinate bis- H_2O complex, whereas free F_{430} at room temperature is 4-coordinate based on the Raman results. Further, the fraction of salt-extracted F_{430} that is 4-coordinate has a Raman spectrum that is distinct from 4-coordinate free F_{430} based on the Raman line frequencies. For example, the 1534- cm^{-1} line of salt-extracted F_{430} is at 1529 cm^{-1} for the diepimer. This difference is probably solely the result of the rearrangement of the substituents at the 12 and 13 positions of the corphinoid macrocycle.

Methyl reductase. The narrowing of the Raman lines of methyl reductase is most likely a result of greater homogeneity at the F_{430} site in the protein environment relative to the solution environment of the F_{430} forms. This indicates a very specific structure for the F_{430} site in the protein.

It is also clear from the large differences in frequency that the chromophore or its environment is unique in some way. The uniqueness may be a result of (1) a novel coordination geometry, (2) an unusual corphinate ligand conformation, or (3) a difference between the structure of the chromophore's peripheral substituents in the native protein and after salt extraction. We have observed that no oxygen, sulfur, or nitrogen ligand complex has come close to giving the frequencies observed for the two strong high frequency lines of methyl reductase. The separation of (1653 - 1575 =) 78 cm^{-1} for methyl reductase is however compatible with either 5- or 6-coordination although so far no ligand examined gives the high frequencies observed for these Raman lines. Thus, the second and third possibilities mentioned above should not be ruled out.

At 77 °K a form similar to the aqueous 6-coordinate form of salt-extracted F_{430} is beginning to make an appearance. At 4 °K the Ni X-ray absorption edge is

similar for methyl reductase and salt-extracted F_{430} (14). Thus, at 4 °K the salt-extracted F_{430} form may predominate in the protein.

Conclusions

The nickel-tetrapyrrole derivative in the methyl-reductase enzyme resides in a unique protein environment. We have not yet been able to find an equivalent structure for F_{430} in solution based on the Raman spectra. Nevertheless, the Raman data suggest that F_{430} in the protein has at least one axial ligand and occupies a site in the protein with a low degree of heterogeneity.

The free form of F_{430} shows evidence of ruffling in that multiple forms are observed in the low temperature Raman spectrum and the species cannot all be ascribed to axial ligand complexes. This low temperature behavior is also noted for the model nickel-corphinoid in non-coordinating solvents such as methylene chloride (5). On the other hand, salt-extracted F_{430} shows no evidence of ruffling, but displays higher affinity for axial ligands than the diepimer.

It is thought that the axial coordination sites of nickel may serve as a binding site for methyl-S-CoM or perhaps the methyl group that is reduced to methane in the reaction. Nickel corphinoids are known to have higher affinity for axial ligands than nickel porphyrins (15) and the unusual affinity may play a role in methane catalysis. The nickel corphinoids also exhibit different behavior in the photolysis of axial ligands than the nickel porphyrins (16). A Ni(I) intermediate may be involved in the reduction of the bound methyl group to methane (17).

Macrocycle flexibility may also play a role in methane catalysis as has been proposed for vitamin B₁₂ (Co-corrin) enzymes involved in biological methyl-transfer reactions (18,19). In these reactions an axial Co-CH₃ complex is known to be an intermediate. Efforts to further elucidate the roles of axial ligation and macrocycle flexibility in the catalytic properties of F_{430} in methyl reductase are continuing using resonance Raman and transient Raman spectroscopic techniques.

Acknowledgements

We thank Professor Albert Eschenmoser for kindly providing the model F_{430} complexes. This work performed at Sandia National Laboratories and supported by the U. S. Department of Energy Contract DE-AC04-76DP00789 and the Gas Research Institute Contract 5082-260-0767.

REFERENCES

1. Wolfe, R. S., Trends Biochem. Sci. 1985, 10, 396.
2. Hartzell, P. L.; Wolfe, R. S., Proc. Natl. Acad. Sci. USA 1986, 83, 6726.
3. Shiemke, A. K.; Scott, R. A.; Shelnutt, J. A., J. Am. Chem. Soc. 1987, submitted.
4. Shelnutt, J. A., J. Am. Chem. Soc. 1987, in press.
5. Shelnutt, J. A. unpublished results.
6. Ellefson, W. L.; Wolfe, R. S., J. Biol. Chem. 1981, 256, 4259.
7. Gunsalus, R. P.; Wolfe, R. S., J. Biol. Chem. 1980, 255, 1891.
8. Pfaltz, A.; Juan, B.; Fassler, A.; Eschenmoser, A.; Jaenchen, R.; Gilles, H. H.; Diekert, G.; Thauer, R. K., Helv. Chim. Acta 1982, 65, 828.
9. Fässler, A.; Pfaltz, A.; Kräutler, B.; Eschenmoser, A., J. Chem. Soc. Chem. Commun. 1984, 1365.
10. Shelnutt, J. A., J. Phys. Chem. 1983, 87, 605.
11. Livingston, D. A.; Pfaltz, A.; Schreiber, J.; Eschenmoser, A.; Ankel-Fuchs, D.; Moll, J.; Jaenchen, R.; Thauer, R. K., Helv. Chim. Acta 1984, 67, 334.

12. Pfaltz, A.; Livingston, D. A.; Jaun, B.; Diekert, G.; Thauer, R. K.; Eschenmoser, A., *Helv. Chim. Acta* 1985, **68**, 1338.
13. Eidsness, M. K.; Sullivan, R. J.; Schwartz, J. R.; Hartzell, P. L.; Wolfe, R. S.; Flank, A.-M.; Cramer, S. P.; Scott, R. A., *J. Am. Chem. Soc.* 1987, in press.
14. Shiemke, A. K.; Scott, R. A., unpublished results.
15. Eschenmoser, A., *Ann. N. Y. Acad. Sci.* 1986, **471**, 108.
16. Ondrias, M. R.; Finsen, E. W.; Crawford, B. A.; Shelnut, J. A., *J. Am. Chem. Soc.* 1987, submitted.
17. Juan, B.; Pfaltz, A., *J. Chem. Soc. Chem. Commun.* 1986, 1327.
18. Wood, J. M. in "B₁₂" Vol 2, ed. Dolphin, D., Wiley: New York, 1982, p.151.
19. Geno, M. K.; Halpern, J., *J. Am. Chem. Soc.* 1987, **109**, 1238.

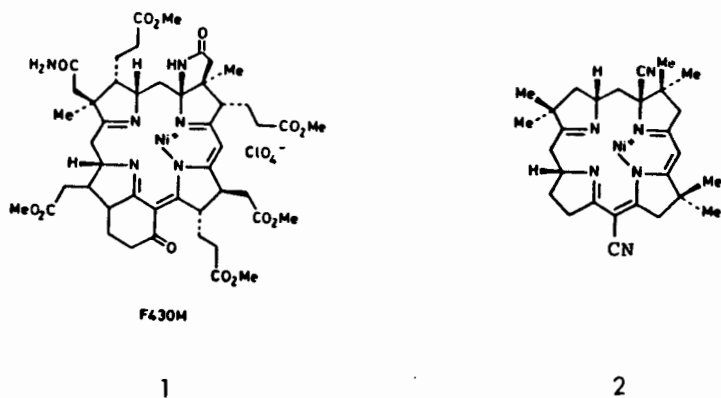


Fig. 1. Structures of F_{430} (1) and the model nickel-corphinoid derivative (2).

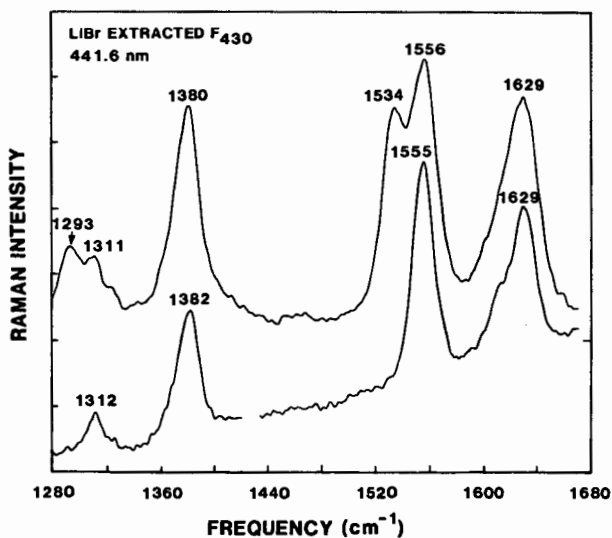


Fig. 2. Resonance Raman spectrum of salt-extracted F_{430} at room temperature (top) and at 77 °K (bottom) in aqueous 10 mM phosphate buffer.

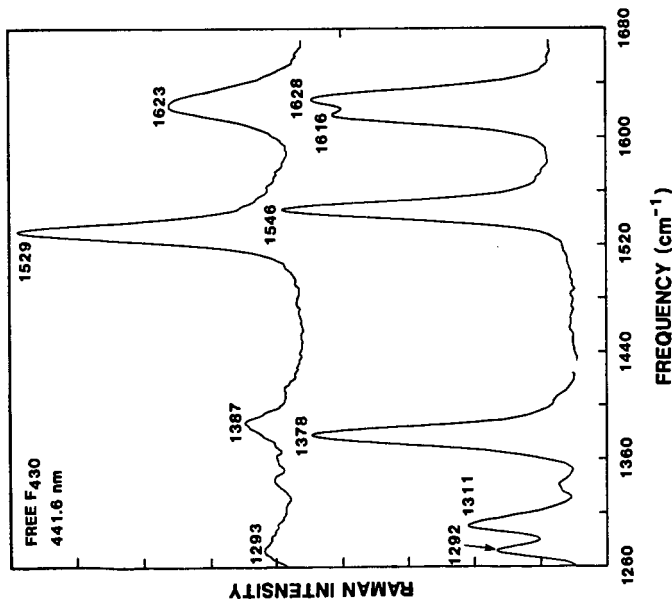


Figure 3. Resonance Raman spectrum of cytosol-free F₄₃₀ at room temperature (top) and at 77°K (bottom) in aqueous 10 nM phosphate buffer.

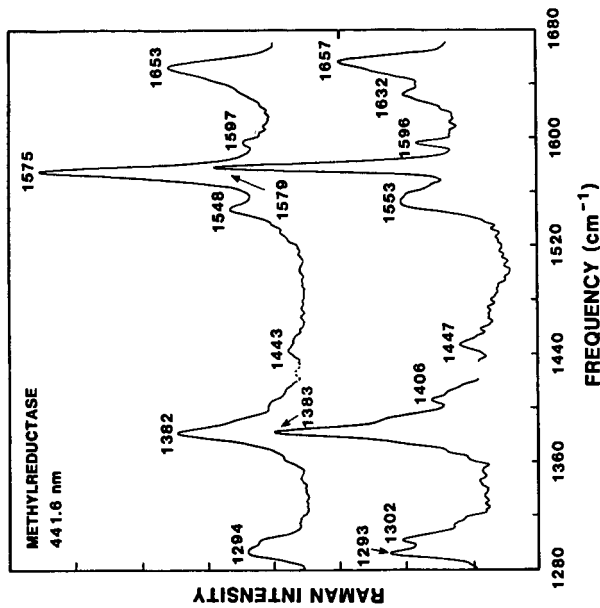


Figure 4. Resonance Raman spectrum of methyl reductase at room temperature (top) and at 77°K (bottom) in aqueous 10 nM phosphate buffer.

THE TESTING OF CATALYSTS FOR ALKANE ACTIVATION*

Frances V. Stohl, John A. Shelnett,
Barry Granoff and Daniel E. Trudell

Sandia National Laboratories, Albuquerque, NM 87185

Introduction

Low oil prices have caused a decrease in the exploration for and development of new oil reserves in the United States. This, combined with an increase in U.S. oil consumption, has resulted in an increased dependence on foreign oil. In June 1986, 40% of the oil used in the U.S. was supplied by foreign sources as compared to 32% in 1983 (1); it is likely that this dependence on foreign oil will continue to increase. This leaves the U.S. vulnerable to sudden, drastic fluctuations in our liquid fuel supply. To minimize this dependence on foreign oil, it is necessary to find new sources for liquid fuels. One potential new source is methane, which makes up about 90% of natural gas. Methane can be partially oxidized to alcohol that could be used directly as liquid fuel or converted to gasoline by Mobil's methanol to gasoline process (2). Economic analyses (3) of potential processes for the conversion of methane to liquid fuel have shown that the use of partial oxidation to form methanol, in contrast to existing conventional methods of forming methanol from syngas, could make a methane to gasoline process economically feasible. Research is needed, however, to find catalysts that are capable of oxidizing methane to methanol with high conversions and high selectivities.

Most work performed on methane partial oxidation has used metal oxide catalysts at high temperatures and pressures (4-6). These studies have shown that catalytic oxidation of methane to methanol is possible, but conversion and selectivity are low. Liu, et. al. (7) have shown that Mo supported on silica is an effective catalyst for the partial oxidation of methane to methanol and formaldehyde when nitrous oxide is present as the oxidant. At a conversion level of 3%, the combined selectivity to CH_3OH and HCHO was 78%, with CO being the principal other product. Using ^3Li -doped MgO at a temperature of approximately 500°C , Driscoll, et. al. (8) were able to show that methyl radicals were formed when methane was passed over the surface of this catalyst. The surface methoxide ions were converted to methanol by reacting with water in the system. The mechanism was similar to the one proposed for the partial oxidation of CH_4 over a Mo/SiO_2 catalyst (7).

Watson and Parshall (9-11) have reported that organolanthanide complexes can react with the C-H bond as shown by isotope exchange reactions using labeled methane. In this case, the catalyst was a dicyclopentadienyl methyltutetium compound. It was proposed that an electrophilic reaction took place between methane and the electron-deficient lanthanide complex.

Janowicz, et. al. (12) have shown that an iridium complex can convert alkanes into hydridoalkylmetal complexes, and that the insertion reaction proceeds through a three-center transition state.

* This work supported by the U.S. Dept. of Energy at Sandia National Laboratories under Contract DE-AC04-76DP00789.

The hydrido products can then be converted to functionalized alkyl halides by treatment with mercuric chloride followed by halogens. Analogous rhodium complexes were shown to undergo similar C-H insertions, but the products were less stable than with the iridium complexes (12). Jones and Feher (13,14) have also shown that alkane C-H bonds can be activated by homogeneous Rh(I) compounds.

Methane can be selectively converted to methanol biochemically via a monooxygenase enzyme (15). Organisms capable of utilizing methane as their sole carbon and energy source are called methanotrophs. In the organism *Methylococcus capsulatus*, the monooxygenase enzyme has been shown to be capable of utilizing a variety of alkanes, alkenes, ethers, alicyclic compounds, etc. (15). The soluble methane monooxygenase from *M. capsulatus* was resolved into three fractions by ion exchange chromatography, but the molecular structures are unknown.

Several other naturally occurring enzymes, such as cytochrome P450 (16), can also catalyze the conversion of alkanes to alcohols at low temperatures and pressures. In an attempt to mimic the activity of these enzymes, we have initiated a program to tailor-make catalysts for the direct conversion of methane to methanol. Our work focuses on the use of metalloporphyrins, and relies on computer-aided design to guide the synthesis of novel catalytic materials. The molecular design techniques are being combined with structural studies (17) of biological catalysts to identify the important characteristics of the active site, the development of activity and selectivity tests to determine structure-activity relationships, and the synthesis of designed catalysts.

Porphyrins are being used because they are present in enzymes that perform C_1 chemistry (methyl reductase, methyl transferase), have versatile structures that can be controlled, and can be synthesized with many different metals. Porphyrins have also shown significant activity for oxidation of long chain alkanes (C_5+) (18,19).

The objective of this paper is to describe the catalyst activity and selectivity tests we are developing and to report on the results of testing several commercially available porphyrins. To get structure-activity relationships, it is necessary to develop several different activity tests using alkanes with varying chain lengths. We started with a cyclohexane test using previously reported conditions (20) so that our results could be compared to literature results. Additional tests we have developed to date use hexane and butane as reactants. In the future, tests will be developed using ethane and methane as reactants.

Experimental Procedures

Materials

The catalysts used in this work included iron tetraphenyl porphyrin ($FeTPPCl$), manganese tetraphenyl porphyrin ($MnTPPCl$) and iron pentafluorophenyl porphyrin ($FeTF_5PPCl$). The first two catalysts were obtained from Porphyrin Products and the third from Aldrich. Methylene chloride (99+) was used as the solvent in all tests. The oxidant was iodosylbenzene (C_6H_5IO) prepared from the reaction of iodosobenzene diacetate with $NaOH$ (21). The alkanes used for the various tests were cyclohexane (99+%), hexane (99%), and butane (99.5%).

Reaction Conditions

Reactions with cyclohexane and hexane were performed in the liquid phase in an argon atmosphere glove-box. Each run had 1.4 cm³ solvent and 0.6 cm³ cyclohexane (or 0.7 cm³ hexane). The ratio of reactant:oxidant:catalyst was 1100:20:1 (20) on a mole basis. These reactions were carried out at atmospheric pressure and ambient temperature (about 30°C in the glove-box) for 2 hours. Reactants were stirred at 1000 rpm.

The oxidation of butane was carried out under 5 psig pressure by bubbling butane₃ at a flow rate of about 12 cm³/min through a solution containing 2 cm³ methylene chloride, 0.005 mmol catalyst, and 0.1 mmol oxidant. A condenser was attached to the reactor to minimize the loss of methylene chloride. The condenser temperature was set at 7°C so that butane condensation did not occur. At this temperature, small quantities of methylene chloride vaporized so that additional solvent was added during the run to maintain constant volume. The reaction temperature was 19°C. After 6 hours, the flow of butane was stopped, the pressure gradually released, and the excess butane was allowed to outgas from the methylene chloride prior to analysis of the products.

Product Analyses

Oxidation products were identified using GC/MS techniques and quantified using capillary column gas chromatographic techniques with commercially available compounds as standards. Product yields are reported on the basis of the amount of oxidant added to the reactor.

Catalyst Characterization

The porphyrins were analyzed using UV-vis spectroscopy. Spectra were taken of both as received and used porphyrins to determine if any degradation of the porphyrin occurred during reaction.

Results and Discussion

Cyclohexane tests were run first in order to compare our results with published values (20). Initial runs used FeTPPCl. Tests with iodobenzene, prepared using previously reported procedures (21), resulted in low cyclohexanol yields, which were thought to be due to a high concentration of contaminants in the oxidant. Infrared (IR) spectra of the oxidant showed the presence of iodobenzene (C₆H₅I). Other phases could not be identified. Extensive cleaning using water and chloroform was carried out; the IR pattern of the product showed a significant decrease in the amount of iodobenzene present. The results we obtained for FeTPPCl and FeTF₂PPCl with this purified batch of oxidant are shown in Table 1. The reported cyclohexanol yields (20) were 10.1% for FeTPPCl and 66.6% for FeTF₂PPCl. Our yields for both porphyrins are significantly higher than the literature values suggesting that we may have prepared a purer oxidant.

An additional test performed with MnTPPCl showed a much greater cyclohexanol yield than obtained with FeTPPCl. UV-vis analyses of the three catalysts before and after reaction showed that the FeTPPCl degraded during reaction, whereas the FeTF₂PPCl and MnTPPCl showed no significant degradation. The extent of FeTPPCl degradation and the cyclohexanol yield from the run with FeTPPCl as a function of time are shown in Figures 1 and 2. A comparison of the results in these two figures indicates that some reaction still occurred even after the porphyrin was completely degraded. A test carried out with

reactant, oxidant and solvent, but no porphyrin, did not yield any cyclohexanol. This indicates that the iron species resulting from the degradation had some activity. The cause of the higher activity of MnTPPCL as compared to FeTPPCL is not definitively known. It could be entirely due to the degradation of the FeTPPCL or could be partially due to FeTPPCL degradation and partially due to differences in the activities of the two metals. This cannot be proven from these runs. Additional studies are being performed to determine the effects of different metals on catalyst activity.

The main structural difference between FeTPPCL and FeTF₂PPCL is the replacement of hydrogens with fluorines on the phenyl rings. Steric and electronic effects of the fluorines prevent catalyst degradation to produce a more stable catalyst. The fluorines may also cause the catalyst to be more active (20). Runs with MnTPPCL and FeTF₂PPCL that were carried out for about 16 hrs did not show any increase in yield beyond the first two hours, suggesting that the reactions might be limited by the amount of oxidant remaining. It has been suggested (20) that the oxidant can be further oxidized by an Fe-oxygen intermediate species of the porphyrin to give iodoxybenzene (C₆H₄IO₂) during these reactions. The iodoxybenzene is not an oxidant. We are currently performing studies to determine the fate of the iodoxybenzene in these reactions.

Activity testing with hexane was performed under the same conditions as with cyclohexane so that yields could be compared. Results for this test are shown in Table 1. The total hexanol yield is lower than the total cyclohexanol yield under the same conditions. The hexanol from the run with FeTF₂PPCL consists of 1% 1-hexanol, 28% 2-hexanol and 27% 3-hexanol. These results show that selectivity to the 1-hexanol is very low and the total yield has decreased in going from the cyclic compound to the straight chain. The decrease in the yield of the 2- plus 3- alcohols in the hexane run, as compared to the cyclohexanol yield with the same catalyst, is proportional to the number of methylene groups. Hexane has 4 secondary carbons whereas cyclohexane has 6, and the yield of 2- plus 3- hexanols is 2/3 of the yield of cyclohexanol.

The run with butane yielded 35% butanol consisting of 34% 2-butanol and 1% 1-butanol. The concentration of butane in the methylene chloride under the test conditions was measured using Raman spectroscopy. The results showed that there was about 8% butane (on a mole basis). This is significantly lower than the 20% hydrocarbon present in the reactions with cyclohexane or hexane. The results of the tests with cyclohexane and hexane cannot be directly compared to the results of the butane tests because of the lower reactant concentration and the differences in reaction times and temperatures. Therefore, additional testing is being carried out to enable this comparison.

Conclusions

The results of the cyclohexane tests carried out for longer times indicate that it is necessary to determine what happens to the oxidant during the reaction, since the results suggest that oxidant is depleted even at low alcohol yields. If a more effective oxidant is found, yields should be significantly higher. The results with butane suggest that we may have a good test procedure for use with shorter chain alkanes. To be able to compare results from tests using cyclohexane and hexane to butane (and to future tests with ethane and methane), it will be necessary to determine the effects of different

reactant concentrations and different reaction times and temperatures.

References

1. Hirsch, R.L., Science 235, 1467, 1987.
2. Williams, R., Oil & Gas J., 76, May 14, 1984.
3. Dautzenberg, F.M., Garten, R.L. and Klingman, G., ACS Division of Ind. Eng. Chem. 21st State-of-the-Art Symposium, Marco Island, Florida, June 15-18, 1986.
4. Foster, N.R., Appl. Catal. 19, 1, 1985.
5. Jones, C.A., Leonard, J.J. and Sofranko, J.A., Energy and Fuels 1, 12, 1987.
6. Sofranko, J.A., Leonard, J.J. and Jones, C.A., J. Catal. 103, 302, 1987.
7. Liu, H.-F., Liu, R.-S., Liew, K.Y., Johnson, R.E. and Lunsford, J.H., J. Am. Chem. Soc. 106, 4117, 1984.
8. Driscoll, D.J., Martin, W., Wang, J.-X. and Lunsford, J.H., J. Am. Chem. Soc. 107, 58, 1985.
9. Watson, P.L. and Parshall, G.W., Acc. Chem. Res. 18, 51, 1985.
10. Watson, P.L., J. Am. Chem. Soc. 105, 6491, 1983.
11. Parshall, G.W., Chemtech, 628, 1984.
12. Janowicz, A.H., Periana, R.A., Buchanan, J.M., Kovac, C.A., Stryker, J.M., Wax, M.J. and Bergman, R.G., Pure and Appl. Chem. 56, 13, 1984.
13. Jones, W.D. and Feher, F.J., J. Am. Chem. Soc. 104, 4240, 1982.
14. Jones, W.D. and Feher, F.J., Organometallics 2, 562, 1983.
15. Woodland, M.P. and Dalton, H.J., Biol. Chem. 259, 53, 1984.
16. Griffin, B.W., Peterson, J.A., and Estabrook, R.W. in "The Porphyrins", ed. Dolphin, D., Academic Press, New York, p.333, 1979.
17. Shelnutt, J.A., Shiemke, A.K. and Scott, R.A. ACS Division of Fuel Chem. Preprints, Aug. 31 - Sep. 4, 1987 (in preparation).
18. Mlodnicka, T., J. Mol. Catal. 36, 205, 1986.
19. Cook, B.R., Reinert, T.J. and Suslick, K.S., J. Am. Chem. Soc. 108, 7281, 1986.
20. Nappa, M.J. and Tolman, C.A., Inorg. Chem. 24(26), 4711, 1985.
21. Saltzman, H., and Sharefkin, J.G., "Org. Synth." 43, 60, 1963.

Table 1. Yields of alcohols reported as a percent of the initial oxidant input to the reactor.

REACTANT	CATALYST	TOTAL YIELD	1-ALC* YIELD	2-ALC YIELD	3-ALC YIELD
Cyclohexane	FeTPPCl	14			
	MnTPPCl	42			
	FeTF ₅ PPCl	84			
Hexane	FeTF ₅ PPCl	56	1	28	27
Butane	FeTF ₅ PPCl	35	1	34	

* ALC = alcohol.

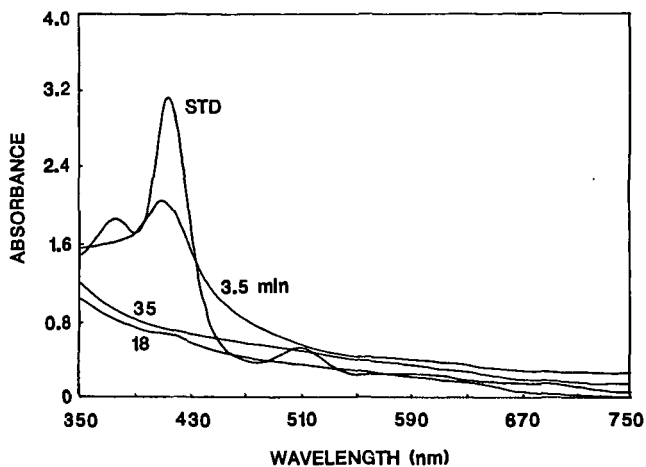


Figure 1. Comparison of UV-vis spectra of FeTPPCl (STD) with catalyst removed (at 3 times) from a reaction with cyclohexane.

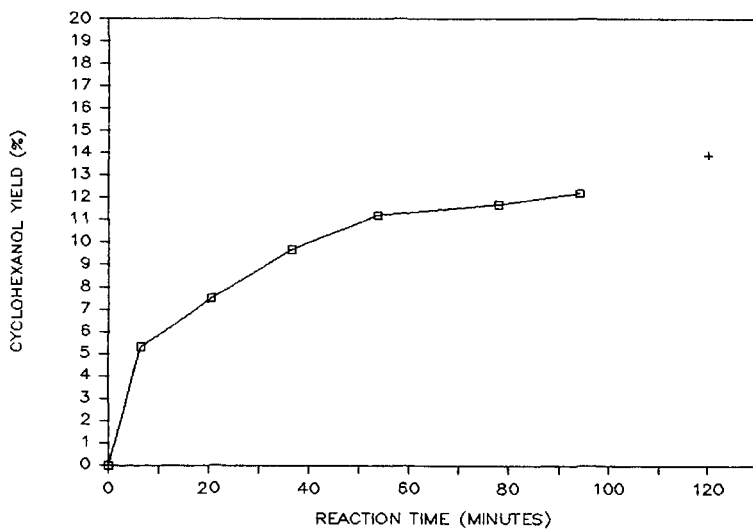


Figure 2. Cyclohexanol yield vs. run time. Catalyst = FeTPPCl. \square = samples pulled from reaction using a syringe (manual injection into GC). + = sample removed from reactor after end of run (automatic injection into GC).

ALKANE ACTIVATION BY OXIDE-SUPPORTED ORGANORHODIUM COMPLEXES

Jeffrey Schwartz

Princeton University
Princeton, NJ 08544

INTRODUCTION

"Homogeneous" catalysis, or catalysis by discrete, soluble transition metal complexes, is dominated by studies of such species in "soft" ligand environments (e.g., consisting of phosphines, sulfides or carbonyls). Historically, one focus of research in this field has been the elucidation of changes in reactivity of a complex which are effected by subtle modification of the ligand environment of the metallic center. It is of interest to us to determine how a gross change in this ligand environment affects the reactivity of a metal system bound to it; specifically, we aim to elucidate changes in rules of molecular reactivity which occur when the "soft" ligand environment of a transition metal complex is replaced by a "hard", oxygen-based one. In this context, solid metallic oxides were chosen to provide this oxygen-based ligation.

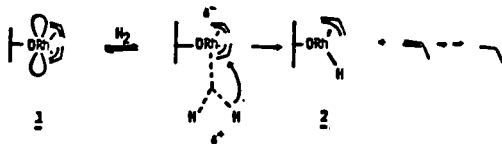
THE CHEMISTRY OF OXIDE-BOUND RHODIUM(ALLYL) COMPLEXES

We chose to focus our attention¹ on the chemistry of oxide-ligated rhodium complexes, given the many interesting and important reactions which exist for this metal in "classical", "soft-ligand"-based homogeneous catalysis. In our work we have used a variety of chemical and spectroscopic procedures to characterize our complexes.

Tris(allyl)rhodium reacts with hydroxyl groups of silica with evolution of 1 equiv of propylene to give Rh(III) species [SiO]Rh(allyl)₂, 1. (We use the terminology "[SiO]" simply to indicate covalent bonding between the oxide and the metal. Details of this interaction are not yet known, although preliminary results of EXAFS studies suggest that several oxygen atoms of the support interact with a given rhodium center.)



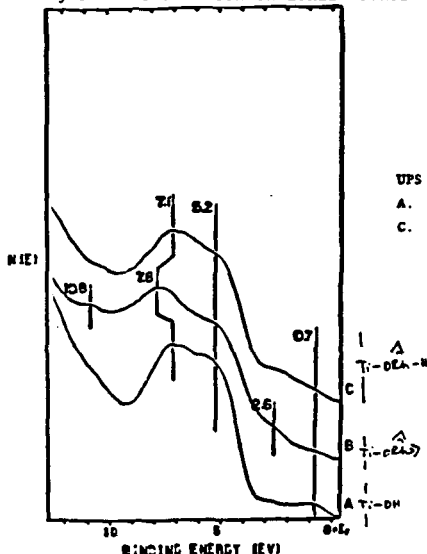
Hydrogen reacts slowly with 1 at room temperature. During this time 1 eq of propane is evolved. Hydrogen uptake measurements correlate with the amount of propane thus obtained and these data are consistent, stoichiometrically, with the formation of [SiO]Rh(allyl)H, 2. The infrared spectrum of 2 shows strong absorptions attributable to the allyl and hydride ligands ($\nu_{\text{Rh-H}} = 2010 \text{ cm}^{-1}$; weaker absorption at 1800 cm^{-1}). If hydrogenation is attempted before chemical deposition has occurred (i.e. before formation of 1 is complete) tris(allyl)rhodium adsorbed on the oxide rapidly reacts to give a black material which shows no infrared transmission, and which may be rhodium metal.



A series of XPS experiments was performed on 2 to corroborate its assignment. A single Rh species was found with an oxidation potential at 308.0 eV (Rh 3d 5/2 vs Si 2p). Thermolysis of this material at 400° followed by XPS analysis revealed

that rhodium metal had been formed (oxidation potential at 307.25 eV). XPS data obtained for 2 falls outside a range of values (308.4 eV to 311.3 eV) which has been determined for Rh(III) salts, a range which overlaps with that for typical Rh(I) complexes (307.6 eV to 309.6 eV). XPS data for covalent organometallic complexes, however, must be interpreted with caution: although 2 is formally a complex of Rh(III), actual positive charge build-up on the metal in this hydride-ligated species may be quite low.

To further probe the nature of the interaction between the metal complex and the oxide support, procedures were developed² for vapor phase deposition of tris(allyl)rhodium onto single crystal hydroxylated TiO₂ in ultra-high vacuum; deposition and a subsequent hydrogenolysis procedure were investigated through a series of UPS measurements made on the surface oxygens of the oxide. These demonstrated that attachment of the bis(allyl)rhodium moiety to TiO₂ was associated with a removal of electron density from the surface oxygens, consistent with the notion that this moiety is a strong electrophile (perhaps stronger than proton). Replacement of one of the allyl ligands by hydride revealed by UPS a build-up of charge on the surface oxygens. Thus the role of hydride as a strong donor ligand toward rhodium, mentioned above in discussions of XPS analyses, is corroborated by these UPS results. Variation in binding energies for surface oxygens as a function of other ligand changes in the coordination sphere of the rhodium demonstrate the covalent nature of the interaction between the metal complex and the oxide, which apparently behaves as a conventional "donor" ligand.



UPS for Rh(allyl)(H) formation on titanium dioxide (001).
 A. 205L water/S' Ar+ B. 2420L tris(allyl)Rh/ (A)
 C. 3230L H₂/(B)

We suggest that coordinatively unsaturated 1 is electrophilic in its reactivity. Activation of H₂ has been observed by aqueous Rh(III) and by numerous metal oxides. In these cases, the concept of "heterolytic" activation of hydrogen has been developed; the coordinatively unsaturated metal center acts as a sink for "H⁻", and a base in the environment of the metal center stabilizes the released proton. When 2 is exposed to D₂, H-D exchange between the atmosphere and residual hydroxyl groups of the silica support is observed, consistent with the notion that in the presence of 2 H₂ or D₂ act as a source of H⁺ or D⁺. Complex 2 also catalyzes rapid (< 1 min) equilibration of 50:50 H₂-D₂ mixture at room temperature.



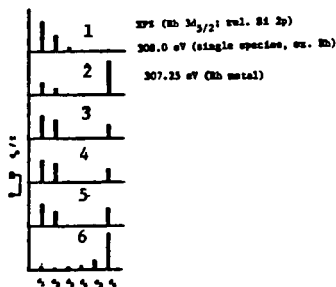
ACTIVATION OF ALKANES

Simple alkanes are conceptual analogs of dihydrogen in that they both should be able to form a two center, three electron bond with an unsaturated metal center utilizing electron pairs in bonding σ orbitals; analogous intramolecular C-H bond coordination is now well established experimentally and has been calculated to be



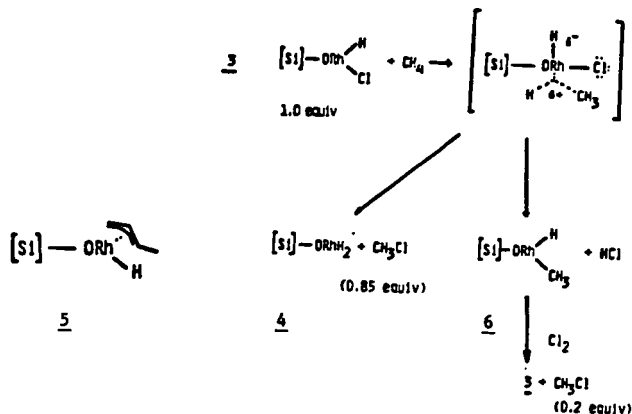
facile intermolecularly. To probe interactions between alkanes and 2, we studied their reaction in the presence of D_2 gas. Sequential H-D exchange occurred when 2 was used to catalyze this process between ethane, for example, and D_2 (see entry 1). Decomposition of 2 (heating at 400° under one atmosphere of hydrogen for 4 hrs) gave a black species which showed no infrared absorptions attributable to Rh-H stretching modes. This species showed catalytic activity for H-D exchange which was different from that of 2: whereas 2 gives rise to a distribution of deuterated ethanes relatively high in d_1 - and low in d_6 -ethane, this other black substance gives rise to a bimodal pattern showing a high degree of d_6 -ethane relative to d_1 (see entry 2). We had noted that simple thermolysis of 2 yields rhodium metal (by XPS analysis) and, therefore, we compared this black material with rhodium on silica obtained by conventional methods. Interestingly, rhodium on silica thus prepared behaves in a fashion similar to that noted for the pyrolysate (see entries 3 and 4).

- (1) -Rh(allyl)H/SiO₂
- (2) Rh/SiO₂ prepared from
-Rh(allyl)H/SiO₂ at 400° , 1 atm H₂
- (3) Rh/SiO₂ prepared from RhCl₃
(aqueous), 400° , 1 atm H₂
- (4) Rh/SiO₂ prepared from RhCl₃
(methanol), 150° , 1 atm H₂
- (5) Rh/KBr prepared from Rh(allyl)₃/KBr,
room temp., 1 atm H₂
- (6) Rh film



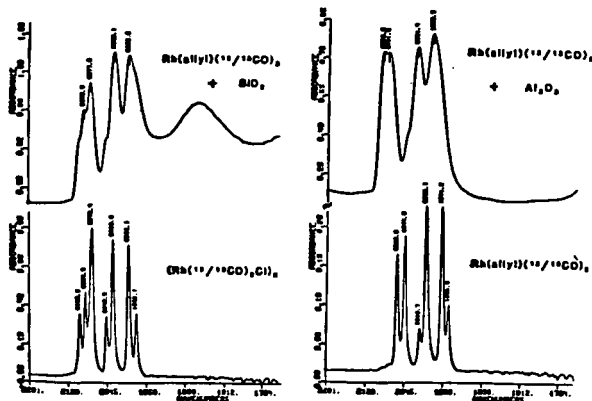
ACTIVATION OF METHANE

We proposed that methane could be activated by an intramolecular ligand rearrangement route from a two-electron, three-centered intermediate analogous to that one proposed for activation of H₂, and we have demonstrated that methane can replace hydrogen in the hydrogen activation step shown in Scheme 2. For example, when 1 is treated with H₂ 2 results; similarly we found that when 1 was treated with methane, a mixture of hydride complexes 2 and 5 were obtained. Hydrogen also reacts with hydrido-chloride complex 3 to give dihydride 4, and therefore 3 was treated with methane. This results in the formation of methyl chloride (0.85 equiv); activation of methane was confirmed by use of ¹³CH₄. Here, infrared analysis performed on rhodium-containing materials showed the presence of dihydride 4, and broadened absorption centered at 2040 cm⁻¹ suggested that 4 could be contaminated with another hydride species, perhaps a (methyl)rhodium(hydride) complex 6; (for the analogous [SiO]Rh(H)Bu, $\nu_{\text{Rh-H}} = 2010 \text{ cm}^{-1}$). Indeed when this material (6) was treated with chlorine, methyl chloride was obtained (0.2 equiv). These observations can be explained³ by the sequences shown below.



OXIDE-DEPENDENT DEPOSITION AGGREGATION

Although we had noted that a variety of oxides could be used for chemical attachment of organorhodium complexes, we had not originally studied how variation in the oxide itself affects the structure or reactivity of complexes bound thereto, and deposition control was attained only by adjusting total content of hydroxyl groups on the oxide. The subtle notion was not considered that relative locations might vary of reactive hydroxyl groups on oxides of different structure, although this distribution of reactive sites would control deposition of one equivalent of an organometallic with regard to another. Silica and alumina are among the most commonly used oxides, in general, for chemical attachment to reactive organometallic complexes, and we found⁴ that an interesting oxide-dependent deposition phenomenon distinguishes these two materials: although for both we utilize samples containing a large excess of acidic hydroxyl groups relative to total rhodium deposited, we note that for silica, deposition of rhodium complexes occurs selectively to generate dimers; on alumina (of comparable total acidity) monomers are formed.



Rhodium carbonyl compounds bound to silica are not structurally stable under hydrogen⁴. This can be demonstrated by noting changes in the infrared spectrum of carbonyl compounds formed on deposition and after subsequent treatment with H₂. Specifically, we note a relative decrease in intensity attributable to terminal carbonyl ligation and an increase in intensity attributable to bridging or "semi-bridging" carbonyl groups. We note that rhodium hydride species (2 or 4) on silica are also structurally unstable under H₂ with regard to clusterification. When these reactions were followed by infrared spectroscopy evidence was obtained for the presence of intermediary molecular hydrogen adducts. Thus, although it is a commonly held assumption that degradation under hydrogen of catalytically active complexes to metallic particles occurs first by reduction of the complex to the metal and then by aggregation, our data suggest that a complementary route, namely aggregation followed by degradation, must also be considered. It is interesting to note that dihydride or dicarbonyl complexes of rhodium bound to either alumina or titanium dioxide do not demonstrate any evidence for analogous clusterification under H₂. Clearly the surface properties of all of these oxides must be better elucidated to understand differences in reactivity imparted to the covalently bound complexes by their various oxide ligands.

1. Alkane Activation by Oxide-Bound Organorhodium Complexes, Schwartz, J. *Acc. Chem. Res.*, 1985, 18, 302-308, and references cited therein.
2. Investigation of a Model Catalytic System in Ultrahigh vacuum: The Adsorption of Rh(allyl)₃ on the TiO₂ (001) Surface, Smith, P.; Bernasek, S. L.; Schwartz, J.; McNulty, G. S. *J. Am. Chem. Soc.* 1986, 108, 5654-5655.
3. Activation of Alkanes by Oxide-Supported Organorhodium Complexes, Kitajima, N.; Schwartz, J. *Proceedings of the Fourth International Symposium on Homogeneous Catalysis - Fundamental Research in Homogeneous Catalysis, Volume III*, 1986, 1003-1014.
4. Oxide-Dependent Deposition and H₂-Promoted Aggregation of Organorhodium Complexes, McNulty, G. S.; Cannon, K.; Schwartz, J. *Inorg. Chem.* 1986, 25, 2919-2922.

Activation of Methane on Iron, Nickel, and Platinum Surfaces.
A Molecular Orbital Study

Alfred B. Anderson and John J. Maloney

Chemistry Department, Case Western Reserve University
Cleveland, Ohio 44106

The activation of alkane CH bonds is the first step in hydrogenolysis and oxidation catalysis. It is clear from simple consideration of metal-hydrogen bond strengths (≈ 250 kJ/mol) and CH bond strengths (434 kJ/mol for breaking the first CH bond in methane) that oxidative addition and not hydrogen atom abstraction will be the route followed on metal surfaces. In contrast, O^- defect centers at oxide surfaces do abstract hydrogen atoms from methane, forming gas phase methyl radicals (1). The greater strength of an OH bond over a CH bond allows this to happen; a molecular orbital analysis has been published recently (2). Though kinetic studies of alkane reactions on metal surfaces are large in number, little is known about catalyst surface composition and structure or the structure and electronic factors responsible for CH activation by metals. The purpose of the present work is to explore mechanisms, activation energies, and orbital interactions associated with the oxidative addition of a methane CH bond to several idealized clean transition metal surfaces.

The metals chosen for our theoretical exploration, iron, nickel, and platinum, have been the topics of several systematic methane catalysis and surface science studies in recent years. A theoretical study of the oxidative addition of methane to an iron surface indicated the reaction was exothermic with an activation energy barrier of roughly 88 kJ/mol (3). In that study, low barriers were also found for dehydrogenation of CH_x ($x=1-3$) fragments and this is reflected in the ability of iron particles to catalyze the high temperature pyrolysis of natural gas to graphite fibers as studied recently by Tibbetts (4). Early work using iron surfaces was unsuccessful in yielding activation energies, probably because contaminants lowered the activity (5).

In the case of nickel, activation energies are higher on single crystal surfaces than on films and supported metal particles. Estimates are 88 kJ/mol on Ni(110) (6), 71 kJ/mol on Ni(111) (7), and 0 (8) and 30 (9) kJ/mol on Ni(100). On a Ni film 42 kJ/mol has been reported (5) and independent studies of methane activation by silica supported nickel yield similar barriers, 29 (10) and 25 (11) kJ/mol.

Activation of n-alkanes on platinum has been studied (12,13). Activation energies are about 46 kJ/mol on Pt(110) (13) and the inactivity of Pt(111) (12) has been interpreted to mean that n-alkane CH activation energies must be greater than 67 kJ/mol (13).

Because of various experimental difficulties in the early work, only the recently determined activation energies, 71 kJ/mol for Ni(111) and 30 kJ/mol for Ni(100) are likely to be accurate (5,9,13). The other values are in greater doubt.

Theoretical Method

The atom superposition and electron delocalization molecular orbital (ASED-MO) method (14) used in this paper is a semiempirical

theoretical approach which uses valence Slater orbitals (15) and experimental ionization potentials (16) as input data. The ASED-MO method is a simple way to predict certain molecular data from atomic data. Its structure and energy predictions are often quite accurate, but in general it is best used to establish and explain chemical trends.

Surfaces were modeled using the bulk-superimposable clusters in Figure 1. Atoms with which methane interacts directly in the transition state are shaded. Adsorption studies were performed assuming high-spin molecular orbital occupations with lower levels in the d band doubly occupied and upper levels singly occupied. The Fe₁₃ and Fe₁₄ clusters had 38 unpaired electrons, the Fe₁₁ cluster 30 and the Ni₁₀ and Pt₁₀ clusters 6 unpaired electrons. The cluster structures are bulk-superimposable and based on well-known lattice constants (17).

Methane activation on Fe(100) and (110) surfaces

Key numerical results are in Table I and transition state structures are in Figure 2. The activation energy for inserting an Fe(100) surface atom into a methane CH bond is 32 kJ/mol and occurs when the bond is stretched 0.36 Å. On a "roughened" surface site, consisting of an Fe ad-atom placed on top in a bulk-like position, the activation energy decreases slightly to 27 kJ/mol. The bonding in the transition state is best characterized as CH donation to the surface and the electronic structure for the ad-atom case is in Figure 3. This figure is representative of all other transition states discussed in this work. The stretching causes one of the 3-fold degenerate t_2 symmetry methane orbitals to become destabilized. Its bending of 22 deg away from the tetrahedral direction contributes further to the destabilization and also causes a small stabilization in one of the other t_2 orbitals. The lowest orbital is destabilized by the distortion. Interactions with the surface consist in a small stabilization of the lowest orbital and mixing of both of the upper orbitals from the t_2 set with the Fe orbitals to form clearly-defined C···H···Fe and C···Fe σ bonding orbitals. The main occupied antibonding counterpart orbital energy lies in the half-filled d band region and participation of the CH σ^* orbital in it removes almost all H contribution; the orbital has a C···Fe σ bonding character.

The transition state structures given in Figure 2 show how the methyl groups are tilted with respect to the two Fe(100) surfaces. The activated CH bonds are bent away from the tetrahedral directions, as are the newly-forming metal-carbon bonds. On these surfaces the deviations from the tetrahedral directions are nearly symmetric; numerical values for structure parameters are in Table I.

The total Mulliken overlap between the atom inserting into the CH bond and the surface cluster decreases when the atom is playing its activating role. Values given in Table I indicate a smaller decrease for the Fe/Fe(100) surface than for Fe(100). Furthermore, the bond order between the adsorbed Fe atom and the surface is less than between a surface atom and its neighbors.

The close-packed Fe(110) surface is much less reactive. The activation energy for site A is 118 kJ/mole and for site B it is 135 kJ/mol - see Figure 2 and Table I. The methyl tilts from vertical are less than for the (100) surface and this is symptomatic of increased steric repulsions with the closely-packed surface. The bending of the

activated CH bond away from the surface is greater than on Fe(100) and the Fe-C bonds are closer to the tetrahedral direction despite the greater Fe-C distances. There are significant changes in the bond order between the activating Fe atom and its neighbors. On the clean surface the bond order is higher than for Fe(100), indicating more near neighbors and stronger bonding. When the iron atom is activating CH, its overlap decreases more than for the (100) surface, lending further support to the idea that activating CH bonds weakens the metal bonding and that the stronger the metal bonding is, the more it must be perturbed and the weaker the activating ability of the surface. This appears to be borne out by the experimental results for (100) and (111) Ni.

Methane activation on Ni(111) and Pt(111) surfaces

Ni(111) is close-packed and the transition state structures are similar to those for Fe(110). The calculated activation energy, 64 kJ/mol, is close to 71 kJ/mol reported in (7), and provides a benchmark for our qualitative numbers. The effect of activation on the overlap of the active Ni atom with its neighbors is the same as for the close-packed Fe(110) surface.

The 43 kJ/mol activation energy calculated for Pt(111) is close to the experimentally determined value of about 46 kJ/mol for the (110) surface (13) and is smaller than implied by early studies of n alkanes on Pt(111) (12). We do not know precisely the reason for the disagreement. The calculations have uncertainty, but it is noted that the effects of transition state methane on the Pt-Pt bond order are more like those for the open Fe(100) surface than the close-packed Fe and Ni surfaces. We also note early work which stated Ni(111) was inactive compared to Ni(110) (6), yet very recent experiments yield a barrier for the Ni(111) surface close to our calculated value. Impurities may have passivated the (111) Ni surfaces in the early work.

Conclusions

The oxidative addition of methane to the iron, nickel, and platinum surfaces considered here is characterized by the insertion of a surface metal atom into a CH bond. Transition state CH bond stretches amount to around 0.4-0.5 Å. In the transition state two methane CH σ orbitals hybridize with the metal s and d band orbitals to form metal-H and metal-C bonds and the antibonding counterpart to these σ donation interactions is stabilized by mixing with the empty CH σ^* orbital to give additional C-metal bond order. Our finding of charge donation to the metal surfaces in most of the transition states conflicts with the conclusions of Saillard and Hoffmann (19) who used stylized structure models and Extended Hückel calculations, but never actually studied properties along reaction paths for activating methane.

We have found that the close-packed iron(110) surface is a much weaker CH activator than the more open (100) surface and that an ad-atom on the (100) surface is the most active site of all. These activities correlate with the inverse of the bond order between the activating surface atom and its neighbors. These bond orders undergo larger absolute and percentage changes when the activation energy is high, indicating a contribution to the barrier comes from a weakening of metal bonding at the transition state. Hydrogen atoms have been noted to weaken iron bonding in clusters while carbon atoms

strengthened iron overlaps (3). It is obvious that adsorption should affect metal bonding. The relative activation of close-packed and open surfaces toward methane could also have been anticipated.

Despite being close-packed, Ni(111) activates methane with a barrier half of that for Fe(110). Our calculated value is in good agreement with recent experiments and experimental estimates for Ni(100) and Ni films are less, as expected from the above theoretical results for iron. Pt(111) is predicted to be more active than Ni(111) and, therefore, much more active than Fe(110). An updated experimental look at Pt(111) is in order.

Acknowledgement

We are grateful to the Gas Research Institute for supporting this research.

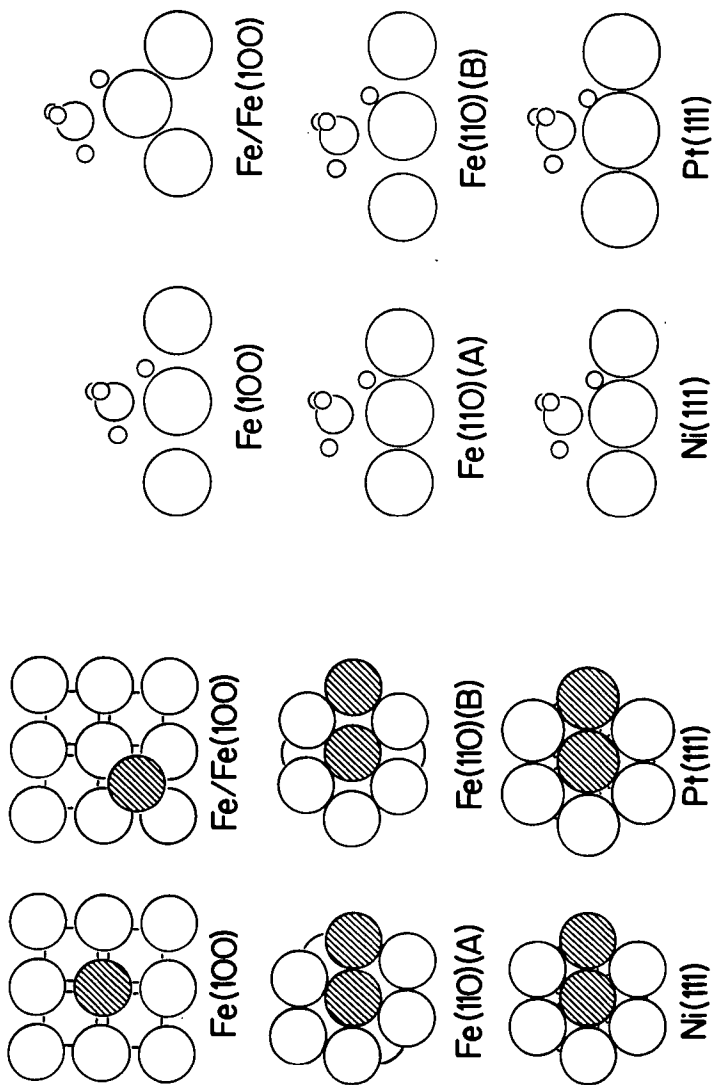
REFERENCES

1. Driscoll, D. J.; Lunsford, J. H. J. Phys. Chem. 1985, **89**, 4415.
2. Mehandru, S. P.; Anderson, A. B.; Brazdil, J. F. J. Phys. Chem. 1987, **00**, 0000.
3. Anderson, A. B. J. Am. Chem. Soc. 1977, **99**, 696.
4. Tibbetts, G. G. J. Cryst. Growth 1984, **66**, 632; 1985, **73**, 431.
5. Wright, P. G.; Ashmore, P. G.; Kemball, C. Trans. Faraday Soc. 1958, **54**, 1692.
6. Schouten, F. C.; Kaleveld, E. W.; Bootsma, G. A. Surf. Sci. 1977, **63**, 460.
7. Lee, M. B.; Yang, Q. Y.; Tang, S. L.; Ceyer, S. T. J. Chem. Phys. 1986, **85**, 1693.
8. Schouten, F. C.; Gijzeman, O. L. J.; Bootsma, G. A. Surf. Sci. 1979, **87**, 1.
9. Hamza, A. V.; Madix, R. J. Surf. Sci. 1987, **179**, 25.
10. Gaidai, N. A.; Babernich, L.; Gucci, L. Kinet. Katal. 1974, **15**, 974.
11. Kuijpers, E. G. M.; Jansen, J. W.; van Dillen, A. J.; Geus, J. W. J. Catal. 1981, **72**, 75.
12. Firment, L. E.; Somorjai, G. A. J. Chem. Phys. 1977, **66**, 2901.
13. Szuromi, P. D.; Engstrom, J. R.; Weinberg, W. H. J. Phys. Chem. 1985, **89**, 2497.
14. Anderson, A. B. J. Chem. Phys. 1975, **62**, 1187.
15. Clementi, E.; Raimondi, D. L. J. Chem. Phys. 1963, **38**, 2868.; Richardson, J. W.; Nieuwpoort, W. C.; Powell, R. R.; Edgell, W. F. J. Chem. Phys. 1962, **36**, 1057; Basch, H.; Gray, H. B. Theoret. Chim. Acta, 1966, **4**, 367.

16. Lotz, W. J. Opt. Soc. Am. 1970, 60, 206; Moore, C. E. Atomic Energy Levels, Natl. Bur. Std. (U.S.) Circ. 467 (U.S. Govt. Printing Office, Washington, D. C., 1958).
17. ASM Metals Reference Book, 2nd ed (American Society for Metals, Metals Park, Ohio, 1984).
18. Saillard, J.-Y.; Hoffmann, R. J. Am. Chem. Soc. 1984, 106, 2006.

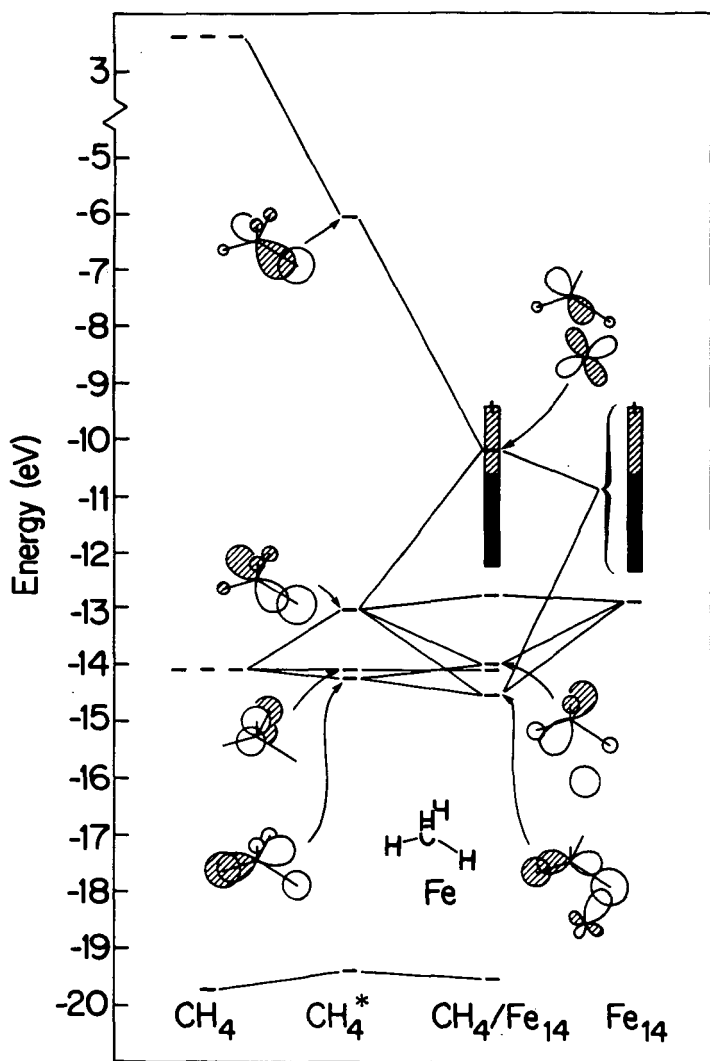
Table I. Calculated transition state properties. Structure parameters are with reference to Figure 2. The CH₃ tilt is from the vertical and bends are from the tetrahedral direction. The C-M bend and M-H and M-C distances are derived; other structure variables were optimized. The M-M_n overlap includes next-neighbor contributions and is calculated in the Mulliken definition.

surface	h _C (Å)	x _C (Å)	CH ₃ tilt (deg)	CH bend (deg)	CM bend (deg)	M-H(Å)	M-C(Å)	M-M _n overlap		E _a (kJ/mol)	
								value	change(%)		
Fe(100)	2.25	0.0	25	22	25	1.65	2.25	2.10	-9	0.36	32
Fe/Fe(100)	2.18	-0.57	37	22	22	1.57	2.25	2.13	-4	0.44	27
Fe(110) (A)	2.35	-0.05	12	34	11	1.66	2.35	2.39	-18	0.46	118
Fe(110) (B)	2.28	-0.30	16	35	8	1.58	2.30	2.37	-18	0.54	135
Ni(111)	2.15	-0.1	12	34	12	1.57	2.15	1.42	-17	0.51	64
Pt(111)	2.30	0.0	15	30	15	1.63	2.30	1.93	-8	0.36	43



1. Cluster models used for the calculations. Shaded atoms are those associated with methane in Figure 2.

2. Calculated transition state structures.



3. Orbital interactions between CH_4 and the ad atom on $\text{Fe}(100)$. Energy levels of distorted methane with the cluster removed are in the CH_4^* column. Orbitals in the shaded metal band region are half-filled.

Conversion of CH_4 into C_2H_2 and C_2H_4 by the Chlorine-Catalyzed Oxidative-Pyrolysis (CCOP) process: I: Oxidative Pyrolysis of CH_3Cl

A. Granada, S.B. Karra, and S.M. Senkan*

Department of Chemical Engineering
Illinois Institute of Technology
Chicago, Illinois 60616

INTRODUCTION:

Methane is available in large quantities in natural gas, thus constitutes an important raw material for the synthesis of higher molecular weight hydrocarbons. Processes exist to convert methane into acetylene, ethylene, and hydrogen using high temperature pyrolysis. However, at the high temperatures needed for the thermal decomposition of methane, the yields of more valuable liquid and gaseous products are too low due to the formation of excessive amounts of carbonaceous solids (see (1) and references therein).

In an earlier patent Gorin (2) proposed a chlorine-catalyzed process in which methane conversion was achieved via CH_4 chlorination, followed by the pyrolysis of chlorinated methanes (CM) and formation of C_2+ products and HCl . The HCl produced can either be converted into chlorine via the well-known Deacon reaction, or can be used to convert CH_4 into CH_3Cl via oxychlorination process, thus completing the catalytic cycle for chlorine. Recently, Benson (3) patented a process similar to that of Gorin (2), in which the flame reactions of Cl_2 and CH_4 were involved. Later, Weissman and Benson (4) studied the kinetics of CH_3Cl pyrolysis.

As expected from bond dissociation energy considerations, the decomposition temperatures for CM would be lower than that for methane, thus the destruction of valuable pyrolysis products, which include acetylene and ethylene would be suppressed. However, in spite of the lower temperatures required for CM pyrolysis, the formation of carbonaceous solids still is a problem (2,4), and this renders the direct pyrolysis of CMs unattractive for practical applications.

The Chlorine-Catalyzed Oxidative-Pyrolysis (CCOP) process developed ameliorates the problem of formation of solid products, while maintaining high yields for acetylene and ethylene (5,6). The CCOP process exploits the high-temperature, non-flame reactions of methane, chlorine, and oxygen, and forms an important bridge between combustion chemistry, halogen inhibition processes (7,8) and chemical reaction engineering. Although some carbon monoxide forms in the CCOP process, CO is a gaseous product thus can be handled easily. In addition, CO can itself be used to synthesize higher molecular hydrocarbons as well.

EXPERIMENTAL:

The experiments were conducted in a 2.1 cm ID quartz tube which was about 100 cm long, and was placed in a 3-zone Lindbergh furnace. A small amount of $\text{CH}_3\text{Cl}/\text{O}_2$ mixture was injected directly into pre-heated argon carrier gas. Experiments were reasonably isothermal as determined by thermocouples. Although laminar flow conditions were present, the deviation

from ideal plug flow behavior was determined to be in the range 10-15%, by the measurements of the concentration profiles in the radial direction.

Species profiles were determined by withdrawing gases through a water-cooled quartz sampling probe positioned centrally at the downstream of the reaction zone, followed by gas analysis by on-line mass spectrometry.

RESULTS AND DISCUSSION:

The experimental conditions investigated are presented in Table I. It should be noted that under these conditions, homogeneous gas-phase kinetics would dominate the reaction processes, with minor contributions from surface induced reactions (4,9).

TABLE I
Experimental Conditions Investigated.
T=980C, P=515 Torr, v=150 cm/s, res. time=50-250 ms

Species	Mixture A		Mixture B	
	Mole percent	CCOP Process	Mole percent	St. Pyrolysis
CH ₃ Cl	7.32		7.47	
O ₂	2.05		-	
Ar	90.6		92.5	

It was possible to conduct experiments with Mixture A indefinitely without any visible signs of formation of solid deposits at the exit of the transparent quartz reactor. Use of mixture B, however, immediately resulted in the formation of dark solid deposits, which rendered the quartz reactor opaque. The formation of solid deposits in the absence of oxygen, however, is an expected result, consistent with the findings of previous investigators (2,4).

In all the experiments the major species quantified, other than the reactants and argon, were: C₂H₂, C₂H₄, C₂H₆, C₂H₃Cl, CH₄, HCl, and CO. Minor species identified, but not quantified were: C₆H₆, H₂O, CO₂, and HCHO.

In Figure 1 the mole percent profile for CH₃Cl and temperature are presented as a function of axial position. In addition, the percent for unaccounted carbon (UC) is also presented. UC is defined as the percent of carbon unaccounted for by the measurements of major gaseous species; thus it represents a measure of extent of formation of solid products.

As seen from the UC profiles in Fig 1, the formation of high molecular weight products, which cannot be quantified by mass spectrometry, is indeed a problem in the absence of O₂. This result is consistent with our qualitative observations noted earlier and the results of Gorin (2), and Weissman and Benson (4).

In Figure 2 the mole percent profiles for HCl, O₂, and CO are presented. The HCl mole percents were calculated from chlorine atom balances, from the measurements of the overall conversion of CH₃Cl, and by assuming that no chlorine is associated with UC. The conversion of O₂ was quite low,

less than about 10%, consistent with the formation of low levels of CO, and by the absence of quantifiable amounts of CO₂ or H₂O.

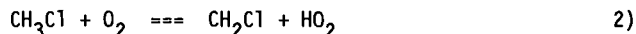
In Figure 3 the profiles for H₂ and CH₄ are presented. The mole fractions for H₂ were obtained from hydrogen atom balances. In Figure 4 the profiles for C₂H₂, C₂H₄, and C₂H₃Cl are shown. These profiles suggest the eventual establishment of pseudo-stationary values for C₂H₂ and C₂H₄ at higher CH₃Cl conversions, consistent with the non-chain character of the process. As seen from these profiles, the levels of these products were not sensitive to O₂.

REACTION MECHANISM:

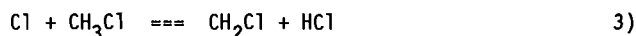
Detailed chemical modeling of the CCOP process suggests that CM pyrolysis starts with the well known initiation step (10):



as well by the following route in the presence of O₂:



These reactions are followed by:

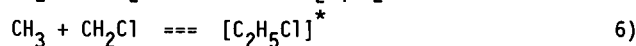
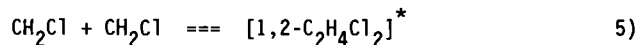


Once formed, HCl undergoes the following fast reaction:



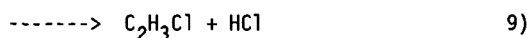
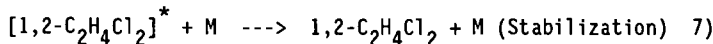
regenerating Cl, and forming CH₄ as an inevitable by-product of CM pyrolysis. Reaction 4 also rapidly consumes the CH₃, therefore rendering CH₂Cl as the most important C₁ radical in the system.

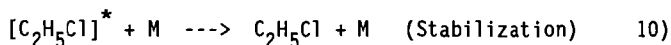
The chemically activated recombination of CH₂Cl, as well as CH₂Cl and CH₃ then determine the major product distributions in the CCOP process. These reactions are the following:



where []* denotes the chemically activated adduct. The CH₃+CH₃=[C₂H₆]* reaction is unimportant because of the lower concentrations of the CH₃ radicals.

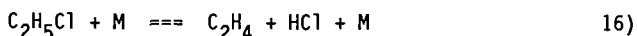
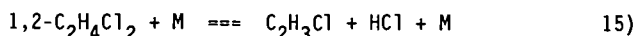
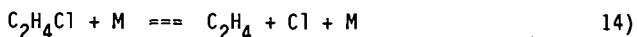
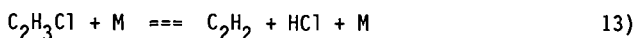
The energized adducts [1,2-C₂H₄Cl₂]*, and [C₂H₅Cl]* then undergo the following parallel stabilization and decomposition reactions:





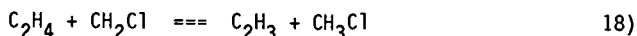
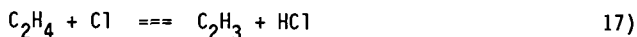
As apparent from these reactions gas density (M) has a significant impact on the nature of the ultimate product distribution. For example, at higher pressures and/or lower temperatures where M is high, collisional stabilization of the chemically activated intermediates is enhanced, thus the formation of recombination products would be favored. Conversely, at low pressures and/or higher temperatures where M is low, HCl and Cl elimination channels would gain greater significance.

These radical combination reactions are then followed by the following, again pressure-dependent, unimolecular reactions leading to the formation of C_2H_2 , and C_2H_4 :



Reaction 13 is the major channel for the formation of C_2H_2 and for the destruction of C_2H_3Cl . The formation of C_2H_4 occurs primarily via reaction 11, and to a lesser extent by reactions 14, and 16.

Ethylene also undergoes the following destruction processes:

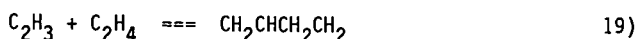


and form one of the most important C_2 radicals in the system, C_2H_3 . Similar destruction channels for C_2H_2 would be too slow to be of any significance.

In the absence of oxygen, the primary reaction pathways available for C_2H_3 are its polymerization:



and to a lesser extent:



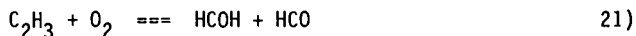
or its highly-endothermic, thus slow decomposition to acetylene:



The $CH_2CHCH_2CH_2$ and $CH_2CHCHCH$ radicals subsequently undergo dehydrogenation, hydrogenation, further addition reactions with C_2H_2 and C_2H_4 , cyclize and ultimately result in the formation of high molecular weight

carbonaceous solids. Although the detailed chemical kinetic steps leading to the formation of solid products are not fully known at present, the process nevertheless is well known to be extremely rapid (11), and reaction 18 is believed to play a pivotal role (4,12, 13).

In the presence of oxygen, however, the C_2H_3 radical has an additional fast reaction channel which effectively competes with the above processes:



This elementary reaction have only recently been isolated and studied (14), and was shown to have no activation energy barrier. Consequently, oxygen has a profound influence on the processes of formation of high molecular weight hydrocarbon solids and carbon by directly intercepting the C_2H_3 radicals. The HCOH and HCO formed by reaction 21 subsequently are converted into CO.

As evident from the above reaction mechanism, although O_2 interrupts the processes that ultimately lead to the formation of solid deposits, it does not directly interfere with the reactions responsible for the formation of ethylene and acetylene. This is supported by the experimental measurements presented in Figure 4, in which the mole percents for C_2H_2 and C_2H_4 remained nearly the same both in the presence and absence of oxygen at the same extent of conversion of CH_3Cl .

It is most important to note that the success of the CCOP process depends on the presence of the following combustion inhibition reaction, which also is the major route for H_2 formation:



Reaction 22, because of its lower activation energy, efficiently removes the H radicals from the system, and renders the following important combustion chain branching reaction:



ineffective in building up the concentrations of O and OH radicals (7,8). Consequently the formation of flames, thus the destruction of CM and valuable products are prevented.

ACKNOWLEDGEMENTS: This research was supported, in part, by funds from the U.S. Environmental Protection Agency, Grant No:R812544-01-0, and the Illinois Institute of Technology.

REFERENCES:

1. Back, M.H., and Back, R.A., in Pyrolysis: Theory and Industrial Practice, Albright, L.F., Crynes, B.L., and Corcoran, W.H., Eds., Academic Press, New York, NY 1983.
2. Gorin, E., US Patent 2,320,274, 1943.
3. Benson, S.W., US Patent 4,199,533, 1980.

4. Weissman, M., and Benson, S., Int. J. Chem. Kinetics., v.16, p.307 (1984).
5. Senkan, S.M. "Production of Higher Molecular Weight Hydrocarbons from Methane", U.S. Patent Application in Progress.
6. Granada, A., Karra, S.B., and Senkan, S.M., Ind. Eng. Chem. Research, submitted, 1987.
7. Chang, W.D., and Senkan, S.M., Combust. Sci. Tech., v.43, p.49 (1985).
8. Chang, W.D., Karra, S.B., and Senkan, S.M., Combust. Sci. Tech., v.43, p.107 (1986).
9. Rotzoll, G., Combust. Sci. Tech., v.47, p.275 (1986).
10. Karra, S.B., and Senkan, S.M., "Detailed chemical kinetic modeling of the CCOP process", manuscript in preparation.
11. Trimm, D.L., in Pyrolysis: Theory and Industrial Practice, Albright, L.F., Crynes, B.L., and Corcoran, W.H., Eds., Academic Press, New York, NY 1983.
12. Frenklach, M., Clary, D.W., Gardiner, W.C., and Stein, S.E., Twentieth Symposium (International) on Combustion, p.887, The Combustion Institute, Pittsburgh 1984.
13. Colket, M.B., Twenty First Symposium (International) on Combustion, The Combustion Institute, Pittsburgh in press 1987.
14. Park, J.Y., Heaven, M.C., and Gutman, D., Chem. Phys. Lett., v.104, p.469 (1984).

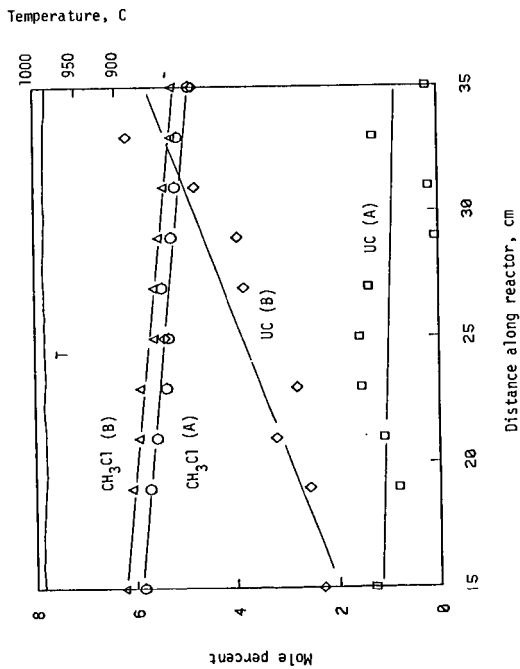


Figure 1. Profiles for CH_3Cl , UC and Temperature.

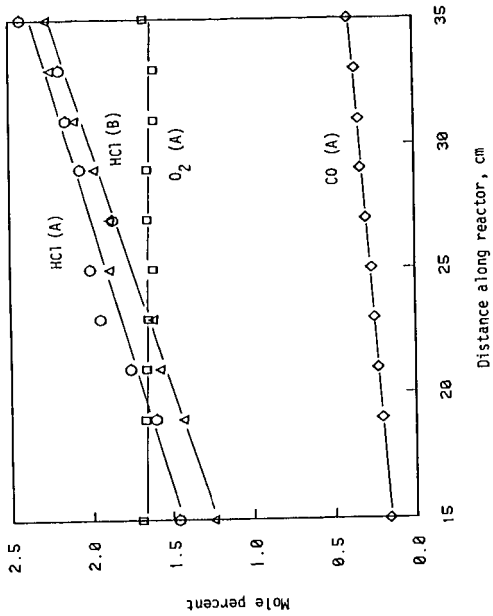


Figure 2. Profiles for HCl, O_2 , CO.

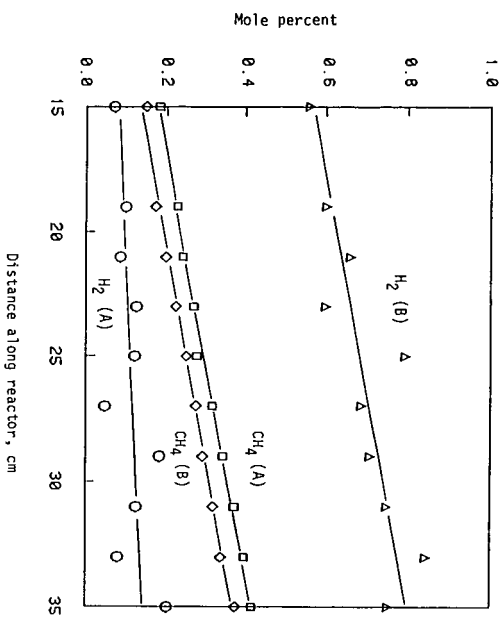


Figure 3. Profiles for H₂ and CH₄.

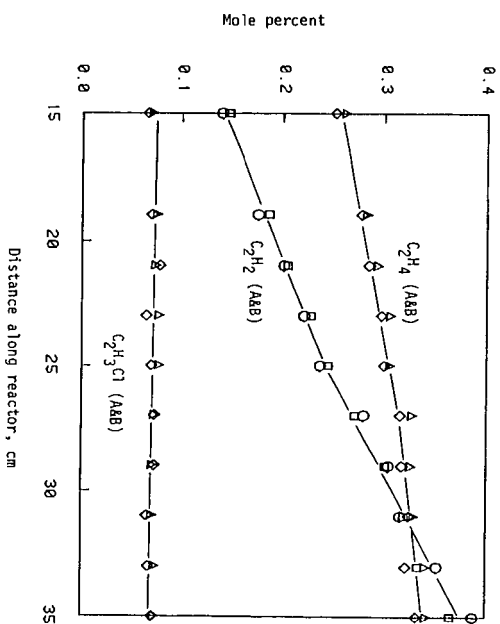


Figure 4. Profiles for C₂H₂, C₂H₄, and C₂H₃Cl.

CONVERSION OF METHANE TO GASOLINE-RANGE HYDROCARBONS

Charles E. Taylor and Richard P. Noceti
U.S. Department of Energy
Pittsburgh Energy Technology Center
P.O. Box 10940
Pittsburgh, PA 15236

Existing processes have been assembled in a novel combination capable of producing higher hydrocarbons from methane with high yield and selectivity. Methane, oxygen, and hydrogen chloride react over an oxyhydrochlorination (OHC) catalyst in the first stage to produce predominantly chloromethane and water. In the second stage, the chloromethane is catalytically converted to higher hydrocarbons, namely, paraffins, cycloparaffins, olefins, and aromatics, by an alumino-silicate zeolite. In the process described, the final hydrocarbon mixture is largely in the gasoline (C_4 - C_{10}) boiling range.

The first stage of the process has been carried out under varying conditions of temperature and residence times. The conversion of reactants, the yields, and the product selectivities are tabulated over the operating range of the catalyst.

The second-stage reaction has been carried out utilizing feeds of chloromethane and various mixtures of chloromethane, dichloromethane, and trichloromethane. A long-term study on a commercial zeolite has shown no significant changes in conversions or product distribution after multiple regeneration cycles.

INTRODUCTION

Current technology for the conversion of methane to more useful compounds includes steam reforming reactions;¹ halogenation;² oxychlorination;³ oxidation, including oxidative coupling and metal oxide reactions;⁴ reaction with superacids;⁵ and various other methods.⁶ At present, these conversion schemes are unattractive because they are marked by low overall carbon conversions or poor selectivities.

In 1975, Mobil Oil Corporation patented a process for the conversion of methanol to higher hydrocarbons by reaction over a zeolite catalyst, such as ZSM-5.⁷ Although later Mobil patents claimed that ZSM-5 would convert any monofunctionalized methane to higher hydrocarbons,⁸ methanol was the feedstock of interest. In 1982, Ione et al.⁹ reported that the conversion products of monofunctionalized methanes over zeolites were independent of the substituent and, for a given catalyst, depended only on the reaction conditions.

In work done at Allied Chemical Corporation, Pieters et al.^{10,11} and Conner et al.^{12,13} reported the selective functionalization of methane by reaction with oxygen and hydrogen chloride over a supported copper chloride catalyst to give tetrachloromethane as the major product. The advantages of the Allied process are significant. Reaction conditions are mild, and conversion and product distribution are stated to be functions of feed stoichiometry and temperature.

If a modification of the OHC reaction conditions produced predominantly chloromethane, a two-step process (Figure 1), in which the chloromethane oligomerization step provides the hydrogen chloride needed for methane chlorination, would be possible. Chlorine, as

hydrogen chloride, is essentially a placeholder in the methylene synthesis. This is the basis of the PETC process.

The work described below demonstrates that an effective method for selective functionalization in combination with oligomerization over a zeolite catalyst provides a facile route for conversion of methane to higher hydrocarbons.

EXPERIMENTAL

The details of the two-stage laboratory reactor system are shown in Figure 2. All the reactants were introduced at slightly above atmospheric pressure from gas cylinders. Flow rates were controlled by a Brooks four-channel mass-flow controller. The feed stream for the first-stage reactor was sampled before and after the experimental run, while the product stream was continuously sampled on line during the run to obtain a mass balance around the OHC reaction. A quadrupole mass spectrometer was used to analyze the feed and product streams. Oligomerization reaction products were collected at dry ice temperatures and analyzed on a Hewlett-Packard 5880 capillary column gas chromatograph equipped with a Hewlett-Packard 5970 mass selective detector (GC/MSD).

Thermogravimetric (TG) measurements were conducted using a Perkin-Elmer TGS-2 system. Differential Scanning Calorimetry (DSC) measurements were conducted using a Perkin-Elmer DSC-2C calorimeter. Both the TG and the DSC were connected to a TADS data station. Heating rates of $10^{\circ}\text{C min}^{-1}$ were employed for 3-6 mg of activated OHC catalyst contained in a gold pan under an inert atmosphere.

The catalysts were contained between quartz wool plugs within horizontal 1- X 35- centimeter quartz tubes enclosed in split tube furnaces. Temperatures were controlled by a feedback controller.

The reactants were preheated to 175°C before entering the catalyst zone. The effluent stream was maintained at 150°C to prevent product condensation before the cold trap or in the capillary inlet to the mass spectrometer.

The oxyhydrochlorination catalyst was prepared according to the literature^{10,11} by sequential layering of CuCl , KCl , and LaCl_3 onto a fumed silica support in nonaqueous solvents. The OHC catalyst was activated in a stream of hydrogen chloride at 300°C for ten minutes prior to use. The ZSM-5 was obtained from Mobil Oil Corporation in the ammonium form with a silica-to-alumina ratio of 70:1. The ammonium form was converted to the acid form by calcining in air at 538°C for 16 hours. The iron-promoted ZSM-5, prepared according to the method of Rao and Gormley,¹⁴ contained 14.5% iron by weight and had a silica-to-alumina ratio of 27:1.

The reaction conditions for the oligomerization of chloromethane were similar to those reported for methanol,¹⁵ i.e., reaction temperature of 350°C and $\text{WHSV} = 1$, using 1 gram of catalyst.

The zeolite catalyst was regenerated by exposure to oxygen at temperatures between 350° and 550°C until the presence of carbon dioxide in the effluent stream was no longer detected by the mass spectrometer. Removal of carbon restored the catalyst to its initial activity even after 14 cycles.

RESULTS

Conversion of methane to chloromethane

The conversion of methane to chloromethane has been observed under various reaction conditions. The data (Table I and Figure 3) show a material balance around 100% and display several trends. Note that methane conversion and polychlorination both increase as residence time and temperature increase.

The highest level of methane conversion occurred around 345°C, which is in the neighborhood of reported eutectic melting points for several CuCl-KCl-LaCl₃ mixtures.¹¹ When the temperature exceeded 350°C, conversion decreased. The DSC measurements showed an endotherm with an onset at 385°C and a maximum at 406°C. The maximum corresponds to the reported melting point of the supported CuCl-KCl-LaCl₃ layers.¹³ The loss of activity occurs well below the experimentally determined melting point and may be explained as the result of a surface area decrease because of phase transitions in the supported phase or a loss of stratification due to diffusion.

Production of carbon dioxide and formic acid, undesirable by-products, also varied with residence time and temperature. As either the residence time or temperature increased, the amount of carbon dioxide increased while the amount of formic acid decreased. Carbon monoxide was not detected in the product stream.

The OHC catalyst is also susceptible to deactivation by exposure to oxygen in the absence of methane at temperatures greater than 100°C. Reactivation requires exposure of the catalyst to hydrogen gas at temperatures between 280° and 300°C. The catalyst is stable in air at ambient temperatures but is hygroscopic. Surface moisture is indicated by a color change from brown to green. Removal of water from hydrated catalyst by heating above 100°C in an inert gas stream gave a catalyst with less OHC activity than freshly prepared and activated catalyst.

Conversion of chloromethane to gasoline

Conversion of chloromethane over ZSM-5 to gasoline-range hydrocarbons has been observed to occur under conditions similar to those for the conversion of methanol. Two forms of the oligomerization catalyst were used in this study. One was a sample of iron-promoted ZSM-5 synthesized in our laboratory; the other was a sample of H-ZSM-5 obtained from Mobil Oil Corporation. Both catalysts produced similar products under the same reaction conditions. The gas chromatograms of the products collected from methanol or chloromethane oligomerization over ZSM-5 are shown in Figures 4 and 5, respectively. The mass selective detector allowed identification of most of the components in the samples, which are listed in Table II. Generally, the products contain ten carbons or less, and a large fraction of the product is aromatic. The presence of chlorinated aromatics was not observed for any of the oligomerization reactions conducted.

Trace amounts of 2-chloropropane and 2-chlorobutane were also found in one of the chloromethane oligomerization products. We hypothesized that these compounds had been formed by vapor phase addition of hydrogen chloride to propene and butene, products of chloromethane oligomerization. This type of addition has been reported to occur under similar conditions.¹⁶ It was further proposed that if these

chlorinated alkanes came in contact with the zeolite catalyst, they would be oligomerized. To test the latter theory, several primary, secondary, and tertiary chlorocompounds of propane, butane, and pentane were allowed to react over ZSM-5 at the conditions for chloromethane oligomerization. In each case, the halocarbon was converted to aromatic hydrocarbons and hydrogen chloride, confirming our hypothesis.

Key to the PETC process is the ability of the ZSM-5 to convert mixtures of chloromethanes, especially those with compositions similar to the OHC product stream, without excessive deactivation due to coking. To determine the effect of feed composition on catalyst coking, mixtures of chloromethane, dichloromethane, and trichloromethane, including one with molar ratios identical to the OHC product stream (Table I, 5.14 seconds), were reacted over ZSM-5. Conversions and coke formation on the zeolite were comparable to those experienced for straight chloromethane (Figure 6) when the molar ratio of chloromethane to dichloromethane was at least 2.75 to 1 and the trichloromethane was 2.3 mole percent or less.

The effects of catalyst aging, caused by prolonged contact of the ZSM-5 with the products of reaction, mainly hydrogen chloride, have been addressed. Conversion studies were undertaken on a single 1-gram ZSM-5 sample exposed to various mixtures of chloromethane, dichloromethane, and trichloromethane under reaction conditions. When conversions dropped below 50%, the zeolite was regenerated by removal of the coke as described above. After regeneration, the initial conversion of chloromethane returned to ~100%. Product distribution exhibited no noticeable change during 800 hours of operation and 14 regeneration cycles.

Conclusion

Methane has been converted to higher hydrocarbons boiling in the gasoline range by the two-stage process described. In the first stage, mixtures of chloromethane, dichloromethane, and trichloromethane were produced by the OHC catalyst in ratios dependent on reaction temperature, residence time, and large changes in feed stoichiometry. Under the conditions described, the ratio of chloromethane to dichloromethane varied from 3.82 to 1.70 as residence time increased from 4.20 to 9.58 seconds. These experiments were conducted at a reaction temperature producing maximum methane conversion. Chloroform production also increased with increasing residence time. Tetrachloromethane formation was at or below detectability limits during all experiments.

The oligomerization of chloromethane to gasoline-boiling-range hydrocarbons occurred under conditions identical to those for methanol. Hydrogen chloride, the by-product of oligomerization, is recoverable from the product stream and may be recycled for use in the OHC step. Mixtures of chloromethane and dichloromethane in ratios of greater than 2.75 to 1, respectively, along with mixtures of chloromethane, dichloromethane, and trichloromethane in the same molar ratios as produced in the oxyhydrochlorination stage, are also oligomerized by ZSM-5. The oligomerization of the mixtures containing the polychlorinated methanes occurs without observable difference in conversion or coke deposition from that experienced for chloromethane or methanol. Long-term exposure of the zeolite to hydrogen chloride and multiple regenerations do not appear to affect either conversions or product distribution.

ACKNOWLEDGMENT

We would like to acknowledge the technical assistance of Dr. Karl T. Schroeder with the GC/MSD analysis, Dr. Sheila W. Hedges with the TG and DSC analyses, and Mr. Richard R. Anderson with the mass spectrometer.

DISCLAIMER

Reference in this report to any specific commercial product, process, or service is to facilitate understanding and does not necessarily imply its endorsement or favoring by the United States Department of Energy.

REFERENCES

- 1 Van Hook, J.P. Catal. Rev.-Sci. Eng. **1980**, 21(1), 1.
- 2 Fontana, C.M.; Gorin, E. U.S. Patent 2 575 167, 1951.
- 3 Kroenke, W.J.; Nicholas, P.P. U.S. Patent 4 467 127, 1984.
- 4 Pitchai, R.; Klier, K. Chem. Rev. **1986**, 28(1), 13.
- 5 Olah, G.A.; Gupta, B.; Farina, M.; Felberg, J.D.; Ip, W.M.; Husian, A.; Karpeles, R.; Lammertsma, K.; Melhotra, A.K.; Trivedi, N.J. J. Am. Chem. Soc. **1985**, 107, 7097.
- 6 Benson, S.W. U.S. Patent 4 199 533, 1980
- 7 Chang, C.D.; Silvestri, A.J.; Smith, R.L. U.S. Patent 3 928 483, 1975.
- 8 Chang, C.D.; Silvestri, A.J.; Smith, R.L. U.S. Patent 3 894 105, 1975.
- 9 Ione, K.G.; Stepanov, V.G.; Romannikov, V.N.; Shepelev, S.E. Khim. Tverd. Topl. **1982**, 16(6), 35.
- 10 Pieters, W.J.M.; Carlson, E.J.; Gates, E.; Conner, W.C., Jr. U.S. Patent 4 123 389, 1978.
- 11 Pieters, W.J.M.; Conner, W.C., Jr.; Carlson, E.J. Appl. Cat. **1984**, 11, 35.
- 12 Conner, W.C., Jr.; Pieters, W.J.M.; Gates, W.; Wilkalis, J.E. Appl. Cat. **1984**, 11, 49.
- 13 Conner, W.C., Jr.; Pieters, W.J.M.; Signorelli, A.J. Appl. Cat. **1984**, 11, 59.
- 14 Rao, V.U.S.; Gormley, R.J. Hydrocarbon Processing **1980**, 59(11), 139.
- 15 Chang, Clarence D. Hydrocarbons from Methanol; Marcel Dekker, Inc.: New York, 1983; Chapter 3.
- 16 Tierney, J.; Costello, F.; Dalton, D.R. J. Org. Chem. **1986**, 11, 5191.

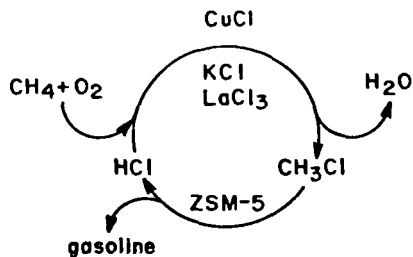


FIGURE 1. CYCLIC PATHWAY FOR THE CONVERSION OF METHANE TO GASOLINE BY THE TWO-STAGE PETC PROCESS

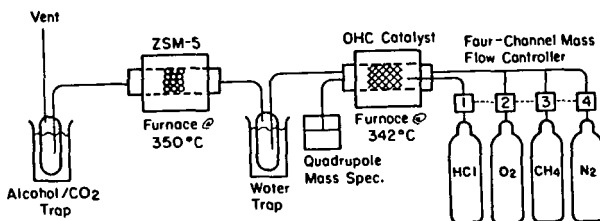


FIGURE 2. LABORATORY-SCALE UNIT FOR THE CONVERSION OF METHANE TO GASOLINE

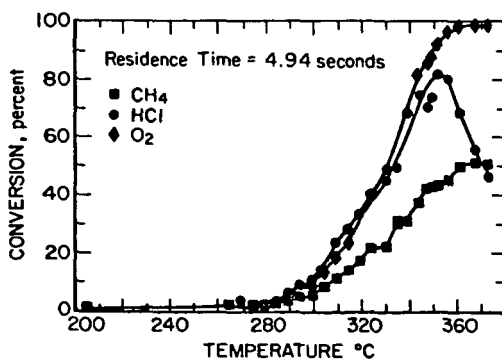


FIGURE 3. CONVERSION OF OXYHYDROCHLORINATION REACTANTS AS A FUNCTION OF TEMPERATURE

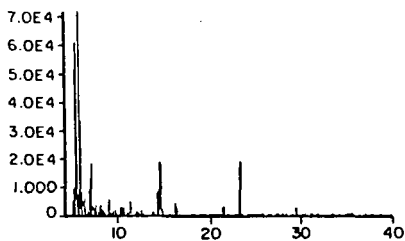


FIGURE 4. GAS CHROMATOGRAM OF METHANOL OLIGOMERIZATION PRODUCTS

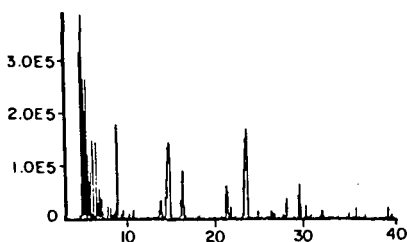


FIGURE 5. GAS CHROMATOGRAM OF CHLOROMETHANE OLIGOMERIZATION PRODUCTS

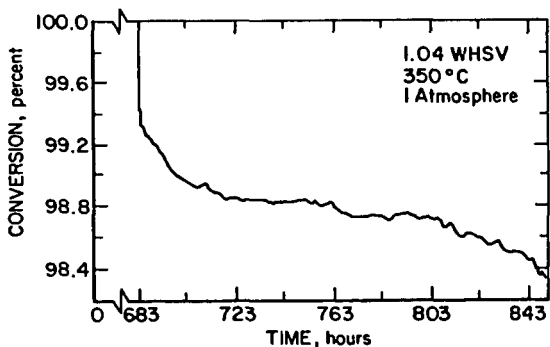


FIGURE 6. CHLOROMETHANE CONVERSION AS A FUNCTION OF TIME AFTER THE 14TH REGENERATION

TABLE I
Selectivity of the OHC Reaction at 342°C

Calculated Residence Time (Sec) ^a	% Conversion ^b			% Product							
	CH ₄	HCl	O ₂	CH ₃ Cl	CH ₂ Cl ₂	CHCl ₃	CCl ₄	CO	CO ₂	HCOOH	CH ₃ Cl/CH ₂ Cl ₂
4.17	25.20	30.17	34.01	75.32	19.72	1.58	0.00	0.00	0.81	2.57	3.82
5.14	28.36	39.28	38.89	73.96	21.24	1.96	0.00	0.00	0.93	1.90	3.48
8.06	38.36	50.71	55.21	68.42	25.83	2.92	0.01	0.00	1.43	1.39	2.65
6.26	36.36	57.72	57.95	67.90	26.16	2.70	0.00	0.00	1.80	1.64	2.60
6.37	45.25	62.41	62.89	66.70	27.15	3.32	0.01	0.00	1.62	1.19	2.46
7.71	42.12	96.36	97.36	64.90	27.47	3.82	0.01	0.00	2.16	1.62	2.36
9.12	53.48	98.00	92.89	57.34	32.31	5.95	0.02	0.00	3.45	0.93	1.77

^aResidence Time = (catalyst void space)/(total inlet gas flow rate).

^b% Conversion = 100 * ([IN] - [OUT])/[IN].

TABLE II
Oligomerization Product Identification

Retention Time (Min.)	Compound
5.086	Pentane
5.259	Butane
5.356	Benzene
6.255	Cyclonexane
6.638	Hexane
8.980	Toluene
13.763	Xylene
14.645	Xylene
16.352	Xylene
21.716	1,3,5-Trimethylbenzene
23.276	1,2,3 + 1,2,4-Trimethylbenzene
26.020	Tetramethylbenzene
29.506	Durene
32.078	Pentamethylbenzene